Chapter 13

Optically Thick Laser-Induced Plasmas in Spectroscopic Analysis

Fatemeh Rezaei

Additional information is available at the end of the chapter

http://dx.doi.org/10.5772/61941

Abstract

Studies on the plasma physics has been grown over the past few decades as a major research field. The plasma can be produced by different sources such as acr, spark, electric discharge, laser and so on. The spectral radiation of the plasma which acts as its fingerprint, contains valuable information about plasma features. Characterization of plasmas by spectroscopic measurement is a powerful tool for increasing the knowledge and applications of these kinds of radiation sources. Therefore, the spectral diagnostics methods are proposed which are based on measurement of spectral lines intensity, estimation of continuous and absorption radiation, and as well as determination of shifts and halfwiths of the spectrum [1]. The fundamental characteristic parameters of the plasma, i.e., the number densities of plasma species, electron temperature, and as well as particle transport property at each plasma space can be determined by optical emission spectroscopy and utilizing appropriate methods [2]. For accurate evaluation of plasma parameters, its thickness must be thoroughly considered. Generally, the plasmas can be separated into two categories of thin and thick groups. In thin plasmas, the re-absorption of radiation is negligible. Consequently, in spectroscopic analysis, the non-self-absorbed spectral radiation is evaluated by considering the summation of all spectral emissions along the line of sight. In optically thick plasmas, the radiation trapping happens which leads to the self-absorption phenomenon in spectroscopic analysis that is explained with details in below section.

Keywords: Thick plasma, self absorption

1. Introduction

Studies on plasma physics have been grown over the past few decades as a major research field. Plasma can be produced by different sources such as arc, spark, electric discharge, laser, and so on. The spectral radiation of the plasma, which acts as its fingerprint, contains valuable

information about plasma features. Characterization of plasmas by spectroscopic measurement is a powerful tool for increasing the knowledge and applications of these kinds of radiation sources. Therefore, spectral diagnostics methods are proposed which are based on measurements of spectral line intensity, estimation of continuous and absorption radiation, as well as the determination of shifts and half-widths of the spectrum [1]. The fundamental characteristic parameters of the plasma, i.e., the number densities of plasma species, electron temperature, and the particle transport property at each plasma space can be determined by optical emission spectroscopy and by utilizing appropriate methods [2]. For accurate evaluation of plasma parameters, its thickness must be thoroughly considered. Generally, the plasmas can be separated into two categories of thin and thick groups. In thin plasmas, the reabsorption of radiation is negligible. Consequently, in spectroscopic analysis, the non-self-absorbed spectral radiation is evaluated by considering the summation of all spectral emissions along the line of sight. In optically thick plasmas, radiation trapping happens, which leads to the self-absorption phenomenon in spectroscopic analysis that is explained in details in the following section.

2. Self-absorption effect

In thick plasmas, when light is emitted from the interior hot parts of plasma and travels to the outside cold regions, the light may be absorbed by the same sort of emitting atoms and molecules. Consequently, the resultant spectrum in a spectrograph will be weakened so that the plasma itself absorbs its emission. This particular kind of absorption of a light source is called self-absorption. The main error that happens in the evaluation of the plasma parameters is the erosion of the spectral intensity due to self-absorption. This phenomenon results in peak height reduction and growth of spectral line widths. In some cases, absorption in the center of the spectral line is more severe than its sides, so that the self-absorption appears as a self-reversal [3]. Self-reversal happens especially in strong resonance lines and in inhomogeneous thick plasmas. In this case, a central dip is observed in spectral lines due to the cold absorbing atoms from the outer parts of the plasma plume. In most cases, the self-absorption is shown as a height reduction, which will not be well recognized from the shape of the spectrum. Self-absorption is mainly severe for atomic lines with low excitation energies of upper levels or spectral lines with high transition probabilities. Furthermore, resonant lines are particularly influenced by the self-absorption effect.

For the spectroscopic purposes in a reabsorbed plasma, the spectral intensity has a complicated relation with plasma parameters, as well as with emission coefficients. Here, the self-absorption effect is investigated for the laser-induced plasmas in local thermal equilibrium (LTE) condition. The details of optically thick plasma calculations in collisional radiative models is indicated in ref. [4].

Ref. [3] completely investigated the effects of different spectral distributions such as Doppler, resonance, and natural broadening on the magnitude of self-absorption. They focused mainly on self-absorption treatment in arcs and sparks sources. Moreover, they investigated the

influences of uniformly excited sources and non-homogenous sources on the amount of line self-absorption. In this study, most of the attention is concentrated on laser as a plasma sources. In the laser-induced breakdown spectroscopy (LIBS) technique, it is observed that in nearly all strong lines of a spectrum and for concentrations more than approximately 3% in the sample, the plasma can behave as a thick medium [5].

It should be noted that self-absorption can be comprehensively studied for different spectroscopic techniques in all intervals of electromagnetism emission, including gamma and X-ray spectroscopy to radiofrequency region, and it comprises the relativistic synchrotron emission as well. In this chapter, the attention is focused on spectral intervals from UV to IR region and on plasma produced by laser radiation.

Self-absorption coefficient of a particular line is usually defined as the ratio of spectral peak height in the presence of self-absorption to its peak magnitude in the condition without self-absorption as:

$$SA = \frac{I(\lambda_j)}{I_0(\lambda_j)}. \tag{1}$$

or it can be expressed as the ratio of line width as below:

$$\frac{\Delta\lambda}{\Delta\lambda_0} = (SA)^{-0.5}. \tag{2}$$

or as the ratio of integrated intensities by

$$\frac{\bar{I}}{I_0} \approx \frac{I(\lambda_0)\Delta\lambda}{I_0(\lambda_0)\Delta\lambda_0} = (SA)^{0.5}. \tag{3}$$

Several research groups proposed different methods of line ratios [6, 7], duplicating mirror [8], curve of growth (COG) [9–12], and calculation models [13–17] for the identification and evaluation of the self-absorption of the considered spectrum. Then, after diagnostic stages, appropriate corrective methods corrected the self-absorbed spectral line intensities before utilizing them for analytical goals. Finally, they calculated the plasma parameters after suitable correction methods, but some groups used these self-absorbed lines straightly by applying appropriate theoretical models without any correction, in spite of its complicated calculations [4, 18–21].

3. Homogenous plasmas

In homogenous plasmas, it is assumed that the plasma parameters are uniform, i.e. they have the same magnitudes in the entire plasma volume. The main investigated parameters are

electron and species temperatures T, and number densities of all different elements in the plasma n.

The intensity of a particular spectral line along the line profile related to transition between two ionic or atomic levels l and u (lower and upper levels), can be evaluated by radiation transfer equation. This equation describes the radiation intensity changes after passing a distance dl of a plasma by taking into account the contribution of the emission within this distance and emission reduction because of absorption along dl [4]:

$$dI_\lambda = \left(\varepsilon_\lambda - k\left(\lambda\right) I_\lambda\right) dl, \tag{4}$$

where, ε_λ is the emission coefficient in thin plasmas, and $k(\lambda)$ is the absorption coefficient. In this equation, the source function is expressed as:

$$S_\lambda = \frac{\varepsilon_\lambda}{k(\lambda)}. \tag{5}$$

The optical depth or optical thickness is defined as multiplication of absorption coefficient by the geometrical thickness of plasma as $\tau = k(\lambda)dl$.

In a two-level system, by neglecting the stimulated emission, the spectral emission can be calculated by considering the spontaneous emission coefficient (in SI units) as follows:

$$\varepsilon_{spec}(\lambda) = N_u A_{ul} h\nu \, V(\lambda). \tag{6}$$

In the above equation, N_u indicates the number of atoms in the upper level and by assumption of holding the local thermal equilibrium (LTE) condition, it is calculated by Boltzmann distribution function. h is the Plank constant, and ν is the spectral line frequency. Here, for more simplification, it is assumed that the line profile distribution for the emission coefficient and the absorption coefficient is similar as Voigt profile $V(\lambda)$.

The absorption coefficient of the two-level system, in SI units, is explained by taking into account the absorption and induced emission between low and high levels of u and l as:

$$k(\lambda) = \frac{h}{\lambda}(B_{ul} N_l - B_{lu} N_u) V(\lambda). \tag{7}$$

B_{ul} and B_{lu} are Einstein coefficients due to absorption and induced emission, respectively, and they are dependent to spontaneous probability coefficient, A_{ul} by:

$$A_{ul} = \frac{g_l}{g_u} B_{lu} \frac{8\pi h\nu^3}{c^3}, g_u B_{ul} = g_l B_{lu}. \tag{8}$$

where, g_l and g_u are the degeneracy of the lower and upper levels, respectively. c is the light velocity in the vacuum. N_l is atomic density in lower level. Therefore, by substituting the above equations in Eq. (7), the absorption coefficient of the mentioned spectral line can be expressed as:

$$k(\lambda) = \frac{g_u A_{ul} N_{tot} \lambda^2}{8\pi Z} e^{-\frac{E_l}{k_B T}} (1 - e^{-\frac{h\nu}{k_B T}}) V(\lambda). \quad (9)$$

here, E_l is the energy of lower level, N_{tot} is the total number densities of species, T is the plasma temperature, Z is the partition function, and K_B is the Boltzman constant.

It should be mentioned that in the collisional-radiative plasma, the calculation procedure is the same as in LTE model, except that the estimation of number densities are performed by rate equation as mentioned in ref. [4].

In this chapter, at first, some corrective methods will be explained for evaluation of self-absorption coefficient in laser-induced homogeneous plasmas by utilizing suitable experimental and numerical methods. Then, the effect of self-absorption on inhomogoneous plasmas will be discussed. Afterward, the impressive parameters on spectral lines charactristics affected by self-absorption will be expressed.

4. Different corrective methods in homogeneous plasmas

One of the methods for observation of self-absorption in the experiment is bending of calibration curve (or curve of growth) constructed by standard samples at high concentrations. Consequently, the self-absorbed spectral lines must be corrected to reach the condition of thin plasmas for prediction of the accurate magnitude of sample concentration without any reduction in intensity. Therefore, in the following sections, some of the corrective methods proposed by different research groups are mentioned.

4.1. Ratio of two spectral line features (width, peak, and surface)

Amamou et al. [6, 7] calculated the self-absorption for both Gaussian and Lorentzian line profiles with a Simplex algorithm program fitting method [22] in a homogenous laser-produced plasma. They fitted the experimental results with theoretical calculation and then, their expressions for Lorentzian profiles were used for quantification of the transition probabilities, ratios, and the ratios of optical thicknesses as well. They introduced different correction factors by considering the ratio of the peaks, line widths, and surfaces of two spectral lines for both of the considered line profiles. The correction factor for the line height can be evaluated by considering the ratio of peak intensities of spectral lines in case of non-self-absorbed atomic line to the case of the self-absorbed line as follows:

$$F_{\max}^{L} = \frac{I_0^{Thin}}{I_0^{Thick}} = \frac{\tau_0}{1-\exp(-\tau_0)}. \tag{10}$$

As well as by taking into account the FWHM ratios, the correction factor for the line width can be calculated by the following equation:

$$F_{\Delta\lambda}^{L} = \frac{\Delta\lambda_L^{Thin}}{\Delta\lambda_L^{Thick}} = \left(-1 - \frac{\tau_0}{\log([1+\exp(-\tau_0)]/2)}\right)^{-1/2}. \tag{11}$$

For an optical thickness of less than 4, it is assumed that the line surface is proportional to the multiplication of line width by its height. Hence, the correction factor for the line surface can be estimated as:

$$F_{S}^{L} = \frac{S_L^{Thin}}{S_L^{Thick}} = \frac{\tau_0}{1-\exp(-\tau_0)}\left(-1 - \frac{\tau_0}{\log([1+\exp(-\tau_0)]/2)}\right)^{-1/2}. \tag{12}$$

here, τ_0 is the optical thickness at central line wavelength (or maximum of optical thickness). The results of these calculations are obtained from the plasma created by laser irradiation on a silicate solid sample placed in a xenon and hydrogen atmosphere for the various multiples of Si II lines. Figure 1 illustrates the evolution of self-absorption correction factors for the above-mentioned parameters in a Lorentzian distribution.

4.2. Simple theoretical equation

El Sherbini et al. [15] presented a simple relation for correcting the self-absorption effect in a homogenous plasma. This model is applicable when the Stark broadening parameter of selected spectral lines is known, as well as when the plasma electron density is available from experiments.

In this work, the intensity of a spectral line in thick condition (erg.s^{-1}.cm^{-3}) along the line profile due to the transition between two levels (j and i) is expressed by

$$I(\lambda) = \frac{8\pi hc^2}{\lambda_0^5}\frac{n_j}{n_i}\frac{g_i}{g_j}(1-e^{-k(\lambda)l}). \tag{13}$$

Generally, the absorption coefficient k(λ) is described by a Voigt profile, which is convolution of a Lorentzian and a Gaussian distribution. In laser sources plasmas, Lorentzian width is associated with the Stark effect and the Gaussian line width is dominated by the Doppler broadening. In a typical LIBS experiment, the Gaussian contribution of a spectral line width is negligible compared to the Lorentzian component, hence, the optical depth k(λ)l can be calculated by

http://dx.doi.org/10.5772/61941

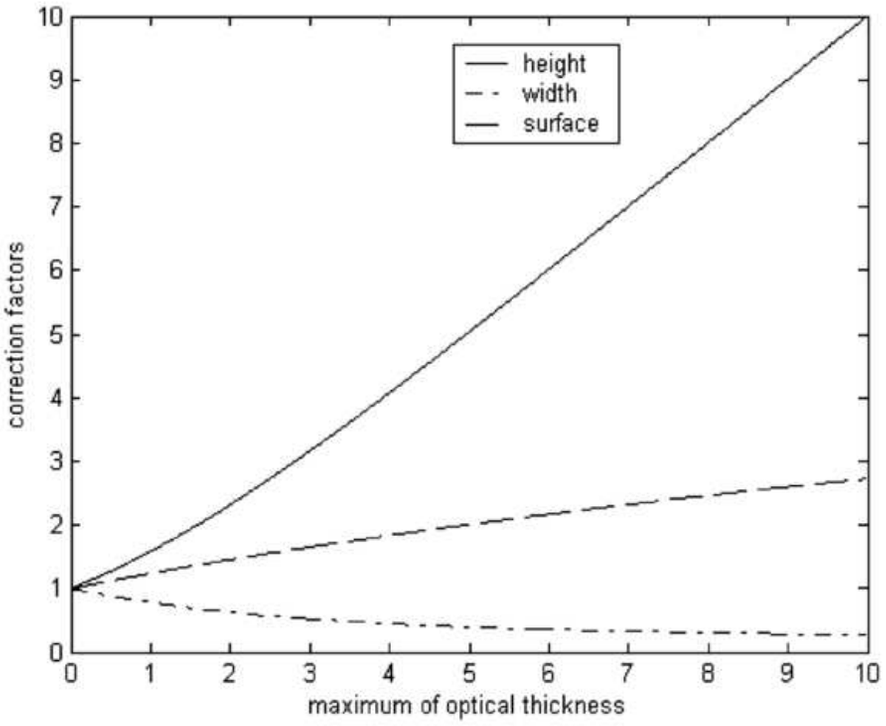

Figure 1. Self-absorption correction factors for: height "solid line", width "alternate dashed line", and surface "long dashed line", in Lorentzian line profile.

$$k(\lambda)l \approx K\frac{\Delta\lambda_0}{4(\lambda-\lambda_0)^2+\Delta\lambda_0^2}, \tag{14}$$

Here, $K = 2\frac{e^2}{mc^2}n_i f \lambda_0^2 l$ and the line width is $\Delta\lambda_0 = \Delta\lambda_L$. In the condition of thin plasmas with $k(\lambda)l \ll 1$, the above equation can be approximated as

$$I_0(\lambda) \approx \frac{8\pi hc^2}{\lambda_0^5}\frac{n_j}{n_i}\frac{g_i}{g_j}k(\lambda)l. \tag{15}$$

Consequently, $I_0(\lambda)$ illustrates the line intensity in case of negligible self-absorption. According to Eqs. (13) and (15), it is clearly seen that, in the case of self-absorption, the line intensity at its peak (i.e. for $\lambda = \lambda_0$) has less value compared to that in the case of thin plasmas. Then, the self-absorption coefficient, SA, can be expressed as

$$\frac{I(\lambda_0)}{I_0(\lambda_0)} = \frac{\left(1-e^{-k(\lambda_0)l}\right)}{k(\lambda_0)l} = \Delta\lambda_0\frac{\left(1-e^{\frac{-K}{\Delta\lambda_0}}\right)}{K} = SA. \tag{16}$$

SA is a coefficient between 0 and 1. SA equals to 1 in the condition of thin plasma and 0 in highly absorbing plasma. Moreover, the line width magnitude is influenced by the self-absorption effect. For obtaining an equation relating FWHM of an optically thick line $\Delta\lambda$ to thin spectral line width $\Delta\lambda_0$ and SA, the following equation can be used:

$$\frac{I(\lambda)}{I(\lambda_0)} = \left(\frac{1 - e^{-K \frac{\Delta\lambda_0}{4(\lambda-\lambda_0)^2 + \Delta\lambda_0^2}}}{1 - e^{-\frac{K}{\Delta\lambda_0}}} \right). \tag{17}$$

By numerically solving the above equation for $\Delta\lambda$ and taking into account the definition of FWHM as $\lambda = \lambda_0 \pm \Delta\lambda / 2$, the intensity of $I(\lambda)$ equals to $I(\lambda_0)/2$. Hence, the exact equation between the measured spectral width ($\Delta\lambda$) and related non-self-absorbed line width ($\Delta\lambda_0$) can be evaluated. Then, after appropriate calculation, provided that $\Delta\lambda$ and n_e are measured from the experiment and w_s magnitude is inserted from the literature, the SA coefficient can be obtained as:

$$SA = \left(\frac{\Delta\lambda}{2\omega} \frac{1}{n_e}\right)^{1/\alpha}. \tag{18}$$

In the above equation, n_e can be measured from the non-self-absorbed spectral line of hydrogen H_α at 656.27 nm. For evaluation of the mentioned method, the experiment is performed on several Al spectral lines radiated from pure aluminum (99.9%) samples. The experiments are done with different equipment, one, at the Physics Department of Cairo University (Egypt) and another, at the Applied Laser Spectroscopy Laboratory in Pisa (Italy). At Cairo University, the experiment is performed with using a single pulse Nd:YAG laser with 160 mJ laser energy, 6 ns pulse duration, and 1064 nm laser wavelength. At Pisa Laboratory, the measurement is done utilizing a mobile double-pulse laser with 8 ns FWHM and laser energy of 80 + 80 mJ with a 2 μs delay between the pulses in collinear configuration.

In Figure 2, the temporal evolutions of the self-absorption coefficients SA for three spectral lines of Al I at 394.4 nm, Al II line at 281.6 nm, and Al II line at 466.3 nm are shown. In this figure, it is seen that the Al I spectral line at 394.4 nm exposes to a higher self-absorption (in the spectra taken at Cairo) compared to the other two cases. This is probably because of the higher electron density (produced by the higher laser energy) so that, based on the Saha equation, it provides a larger amount of neutral atoms in the plasma. Moreover, it is clearly observed that the ionized aluminum lines illustrate a low to moderate self-absorption at later delay times, but they are approximately optically thin for delay times lower than 3 μs. Furthermore, the increase of plasma optical thickness at longer delay times is proved for the Al I spectral line at 394.4 nm and is likely because of the plasma plume cooling which induces a growth in the population of the atomic and ionic lower energy levels.

http://dx.doi.org/10.5772/61941

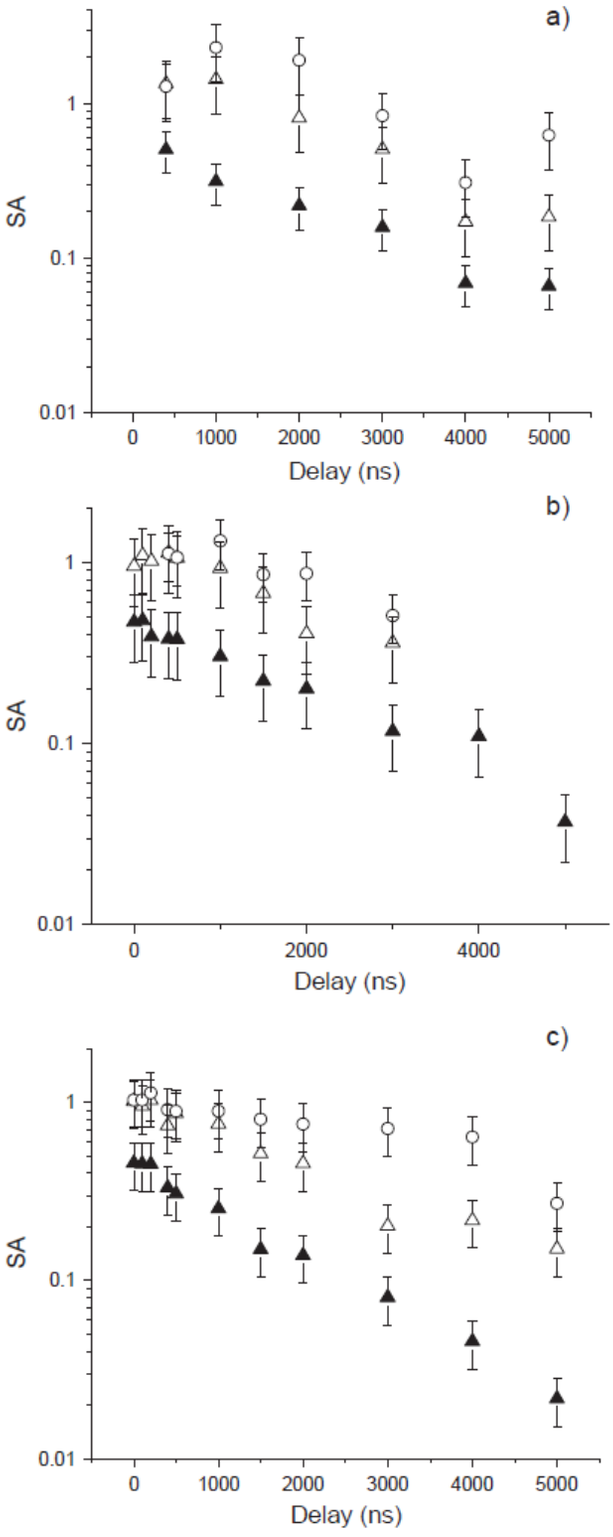

Figure 2. Temporal evolution of self-absorption coefficient SA for Al I spectral line at 394.4 nm (solid triangles), Al II line at 281.6 nm (open triangles), and Al II line at 466.3 nm (open circles). Measurements performed at Cairo University by impact of a single pulse with laser energy of 760 mJ.

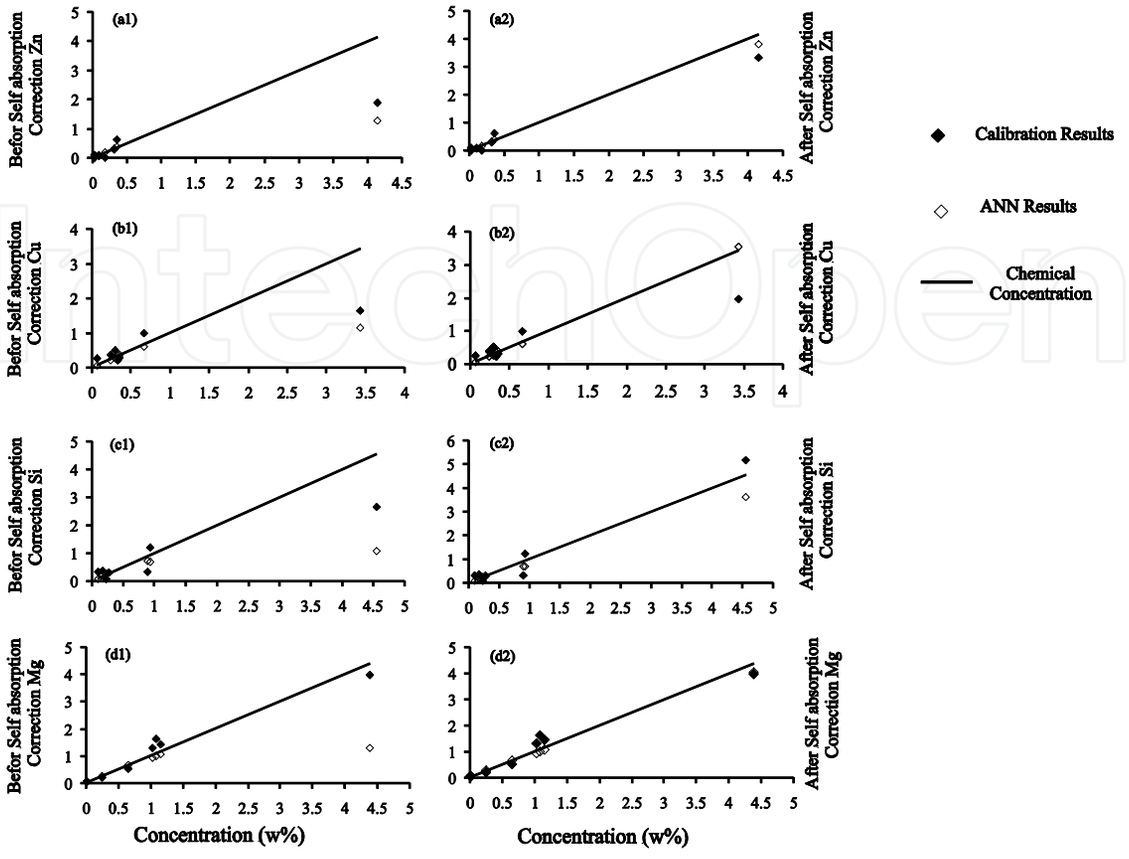

Figure 3. Comparison between the results of ANN and calibration methods with the chemical concentrations (1) without self-absorption correction and (2) with self-absorption correction for the elements of (a) Zn 334.40 nm, (b) Cu 324.40 nm, (c) Si 288.16 nm, and (d) Mg 285.21 nm.

By utilizing the above simple equation, Rezaei et al. [23] corrected the aluminum intensities and then, they predicted the known concentrations in the standard samples with two calibration curves and artificial neural network (ANN) to compare the accuracies of these methods. They used laser-induced breakdown spectroscopy (LIBS) technique for concentration predictions of six elements: Mn, Si, Cu, Fe, Zn, and Mg in seven Al samples. Then, the calibration curve and ANN techniques acquired by six samples are applied for prediction of the elements concentration of the seventh standard sample. In this experiment, a Q-switched Nd:YAG laser at 1,064 nm with a repetition rate of 10 Hz, diagonal output beam of 2.3 mm, and pulse width of 8 ns is focoused on samples. Laser pulse operating at TEM00 mode is adjusted for 50 mJ. The spectra are recorded with an ICCD with exposure time of 1 s and gate width of 5 μs. A comparison between two prediction methods of ANN and calibration curve with their real concentrations in standard samples for four elements of Zn, Cu, Mg, and Si is shown in Figure 3. As it can clearly be seen, at high concentrations, a considerable deviation from real data appeared in Figures 3(a1–d1) in the cases before correcting the self-absorption effect, while when taking into account the self-absorption effect, ANN prediction improves very much in Figures 3(a2–d2). As it is expected, the predictions of the farthest right points on Figure 3, i.e. before considering that self-absorption is not very reliable. Since, these data are a bit greater

than the concentration ranges of the training analysis. Results indicate that after self-absorption correction, and at high concentrations, except for Si, the ANN method illustrates more accurate results with a lower relative error compared to the calibration curve method. These results express that the ANN approach is better than the traditional calibration technique for concentration prediction after self-absorption correction, so that the predicted intensities with ANN are nearer to the real emission spectra. The reason for this fact is that ANN obeys a nonlinear behavior at training stage. Moreover, the used constraint on ANN at the training step causes considerable improvement in its accuracy, while the calibration curve follows a linear function which induces higher errors in its predictions.

4.3. Curve of growth

Curve of growth (COG) method makes a relation between the emission intensity and the optical depth. First, this technique was applied for light sources of resonance vapor lamps [24] and flames [25, 26]. Then, Gornushkin et al. [27] applied a COG method for laser-induced plasma spectroscopy. Recently, Aragon and Aguilera represented several effects of different parameters such as variations of optical depth [11], plasma inhomogeneity [10], and delay time [12] on evolutions of COG curves. They fitted the theoretical COG equations to the experimental results and then, extracted plasma parameters, such as number density of neutral emitting atoms and damping constant. Moreover, they utilized the COG curves for estimation of the magnitude of self-absorption parameter and for the evaluation of the concentration at which transition from thin to thick plasma happens. They proposed that the integrated intensity of a spectral line ($W.m^{-2}.sr^{-1}$) in an optically thick plasma can be calculated from [11]:

$$I = I_P(\nu_0)\int_0^{\infty}(1-e^{-\tau(\nu)})d\nu, \tag{19}$$

where, ν_0 is the central frequency (Hz) of the spectral line, $I_P(\nu_0)$ is the Planck blackbody distribution ($W.m^{-2}.Sr^{-1}.Hz^{-1}$), and $\tau(\nu)$ is the optical depth which in a homogeneous plasma in LTE condition can be expressed as:

$$\tau(\nu) = k'(\nu)l = \frac{e^2}{4\varepsilon_0 mc} N f_{ij} l \frac{g_i e^{-\frac{E_i}{K_B T}}}{Z(T)} \times \left(1 - e^{-\frac{E_j - E_i}{K_B T}}\right) L(\nu), \tag{20}$$

$k'(\nu)$ is the effective absorption coefficient (m^{-1}), which includes the contribution of induced emission and absorption, l is the plasma length (m), f_{ij} is the transition oscillator strength (dimensionless), and $L(\nu)$ is the normalized Voigt line profile (Hz^{-1}) as follows:

$$L(\lambda) = \frac{2(\ln 2/\pi)^{1/2}}{\Delta\nu_D} \frac{a}{\pi} \int_{-\infty}^{+\infty} \frac{e^{-t^2} dt}{(y-t)^2 + a^2}. \tag{21}$$

In Eq. (21), the dimensionless parameters of *y* and a are defined as

$$a = \frac{(\Delta\nu_N + \Delta\nu_L)}{\Delta\nu_D}\sqrt{\ln 2} \approx \frac{\Delta\nu_L}{\Delta\nu_D}\sqrt{\ln 2}. \tag{22}$$

$$\mathrm{y} = \frac{2(\nu - \nu_0)}{\Delta\nu_D}\sqrt{\ln 2}, \tag{23}$$

where, $\Delta\nu_D$ $\Delta\nu_N$ and $\Delta\nu_L$ are are the Doppler, natural and Lorentzian line widths (Hz), respectively. It should be noted that the optical depth of a spectral line depends on the multiplication of $Nf_{ij}l$. The relation between the line intensity I and $Nf_{ij}l$ is expressed by Eq. (19) and is called a curve of growth equation. The main problem in utilizing the LIBS technique for analysis is the complex relation between number densities of emitting species N and the concentration in the sample *x*. In this study, it is assumed that the matrix effects are negligible, so that N is proportional to x by the following equation:

$$N = N^{'}\frac{x}{100}. \tag{24}$$

In the above equation, N indicates the number densities of emitting elements (m^{-3}) in the plasma for the sample which contains 100% concentration. By inserting N in Eq. (24) to Eq. (20), the optical depth can be calculated versus wavelength λ(m) as:

$$\tau(\lambda) = 10^{-2}k_t N' x l L(\lambda). \tag{25}$$

The coefficient k_t, which is dependent to the transition parameters, can be calculated by determination of the plasma temperature as

$$k_t = \frac{e^2\lambda_0^2}{4\varepsilon_0 mc^2} f_{ij}\frac{g_i e^{-\frac{E_i}{K_B T}}}{Z(T)}\left(1 - e^{-\frac{E_j - E_i}{K_B T}}\right). \tag{26}$$

In the above equation, λ_0 is the central wavelength (m), *c* is the light speed in vacuum ($m.s^{-1}$), *e* is the electron charge (C), g_i is degeneracy of lower level, m is electron mass (kg), f_{ij} is the transition oscillator strength (dimensionless), K_B is Boltzmann constant ($J.K^{-1}$), Z(T) is partition function (dimensionless), ε_0 is is the permittivity of free space ($F.m^{-1}$), E_i and E_j are energies of lower and higher levels, respectively. By applying Eq. (26) for the optical depth, the spectral line intensity can be obtained versus the concentration of the emitting element in the sample as below:

http://dx.doi.org/10.5772/61941

$$I(x) = I_P(\lambda_0)\int_0^{\infty}\left(1 - e^{-AxL(\lambda)}\right)d\lambda. \tag{27}$$

A parameter in Eq. (27) is the plasma perpendicular radiating area (m^2), which is defined by

$$A = 10^{-2} k_t N' l. \tag{28}$$

The asymptotic behavior of the COG in low and high concentrations can be obtained by

$$I_{low} \cong I_p A x. \tag{29}$$

and

$$I_{high} \cong I_p \left[2A(\Delta\lambda_L)\right]^{1/2} x^{1/2}. \tag{30}$$

In double logarithmic scale, by considering the entire concentration range, a linear equation can be depicted. The intersection point of the asymptotes shows the following abscissa:

$$x_{\text{int}} = \frac{2\left(\Delta\lambda_L\right)}{A}. \tag{31}$$

This point determines the transition limit from thin to thick plasma and starting of the saturation of the spectral line. For instance, the measured spectral intensities of two neutral Fe lines are depicted versus concentration for the Fe-Ni samples. Here, the experiment is performed by focusing of a Q-switched Nd:YAG laser with 1064 nm wavelength and 4.5 ns line width at 20 Hz repetition rate on Fe-Ni alloy samples in atmospheric air. The pulse energy is adjusted for 100 mJ by utilizing of an optical attenuator. Moreover, the plasma emission is collected with temporal resolution, using a delay time of 5 μs from the laser pulse and a gate width of 1 μs. For comparison, the theoretical results are shown in this figure, too. These curves are illustrated in linear and double-logarithmic scales.

As it is seen in Figure 4 the atomic line at 375.82 nm, which contains a higher value of the k_t coefficient rather than the spectral line at 379.50 nm, exposes to a more intense self-absorption in the LIP experiment, which appears as a nonlinear COG curve at lower concentrations.Then, this group developed COG curves by introducing the CSigma graph [2], which comprises different lines of various elements in similar ionization states for LIBS technique. The method is based on the Saha, Boltzmann, and radiative transfer equations for plasmas in LTE condition. Cσ graphs rely on the evaluation of cross-section of a line, i.e. σ_1 for each of the experimental

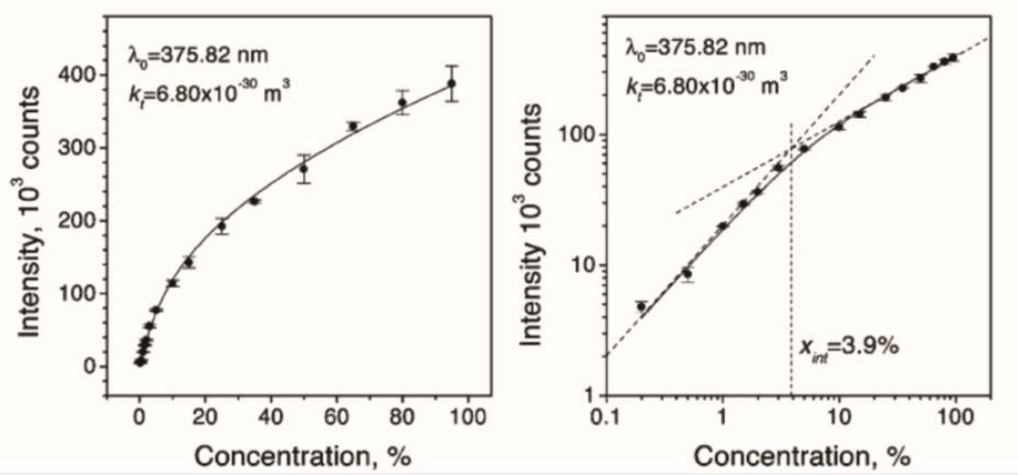

Figure 4. Theoretical and experimental COG for Fe I spectral line on a linear form in left and a double-logarithmic scale on right side. The magnitudes of k_t and x_{int} are indicated in this figure.

results, by knowing the electron density, temperature, and the line atomic data. Then, they fitted the experimental Cσ graphs to calculated curves and four parameters of βA (β is the system instrumental factor equal to the multiplication of the spectral efficiency by the solid angle of detection and A is the transverse area of the plasma region in which the emission is detected), Nl (columnar density), T, N_e could be determined for characterization of LIBS plasma for different ionic and neutral species. The details of the mathematical calculations are expressed in ref. [2].

4.4. Calibration free

Bulajic et al. [14] devised an algorithm for self-absorption correction which was first utilized for three different certified steel NIST samples and for three ternary alloys (Au, Ag, Cu) with known concentrations. Then, it was suggested as a tool for automatic correction of different standardless materials by laser-induced breakdown spectroscopy by using a calibration-free algorithm. The results illustrated that the self-absorption corrected calibration-free method presents reliable conclusions and improves the accuracy by nearly one order of magnitude. The main advantages of applying calibration curve is minimizing the matrix effect, which induces errors in precise evaluation of plasma parameter.

In this work, for each value of SA, 30 different samples are generated. Each synthetical line is appropriately fitted with the analytical software, which yields an estimation value for the parameters $\Delta\lambda_L$ and $\Delta\lambda_G$. In Figure 5, statistical results of $\Delta\lambda_L$ for different values of SA are reported, which explains how, for self-absorbed spectral lines, the experimental Lorentzian width deviates from the 'real' magnitude. Furthermore, by begining from the measured Lorentzian width, it is not feasible to obtain the true value because of the distortion of Voigt profile and the dispersion of the profile of the calculated line widths. It is found more reliable methods for acquiring the true spectral Lorentzian width, by starting from the total line width (i.e. Gaussian plus Lorentzian), which is proved to depend on the SA parameter based on the following expression (see Demtroder [28]):

http://dx.doi.org/10.5772/61941

$$\Delta\lambda_{obs} = \frac{\Delta\lambda_{true}}{\sqrt{SA}} \approx \frac{\sqrt{\Delta\lambda_L^2 + \Delta\lambda_G^2}}{\sqrt{SA}}. \tag{32}$$

Actually, a very good agreement is seen between the values of the total broadening quantities calculated according to the fit of the simulated self-absorbed profiles and those calculated by Eq. (32), when the magnitude of $\Delta\lambda_{true}$ is known. Hence, by assumption of knowing the self-absorption coefficient SA, the total true width can easily be found by utilizing Eq. (32), and then, the contribution of Doppler broadening $\Delta\lambda_G$ and instrumental broadening $\Delta\lambda_L$ will be obtained.

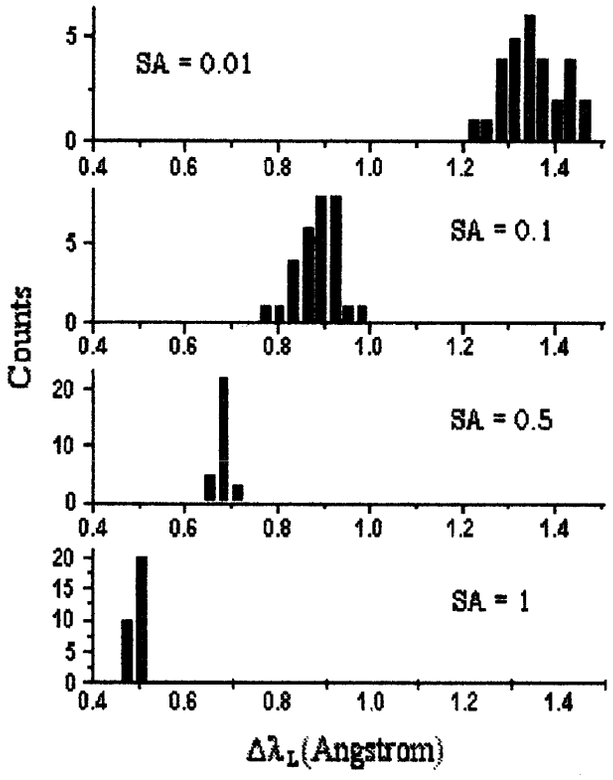

Figure 5. Statistical analysis of Lorentzian width magnitudes attained by fitting with simulated lines with $\Delta\lambda_L$ and $\Delta\lambda_G$ fixed to 0.5 and 0.1 A, respectively, for spectral line of Cu at 324.7 nm, and SA are 1, 0.5, 0.1, and 0.01 from the bottom.

Moreover, Figure 6 illustrates the simulation result of the copper line profile at 324.7 nm at different values of self-absorption for comparing with precious alloy sample containing 40% of Cu. Here, the simulation is performed by curve of growth method as mentioned before. In this figure, the 'flat-top' shape, which is a representation of the self-absorption effect, is clearly seen. Since the peak height reduction can't be well recognized as self-absorption effect, an algorithm is developed for automatic evaluation of self-absorption phenomenon. The performance of self-absorption correction is presented into the CF-LIBS procedure with a recursive algorithm, which is shown by a diagram in mentioned reference.

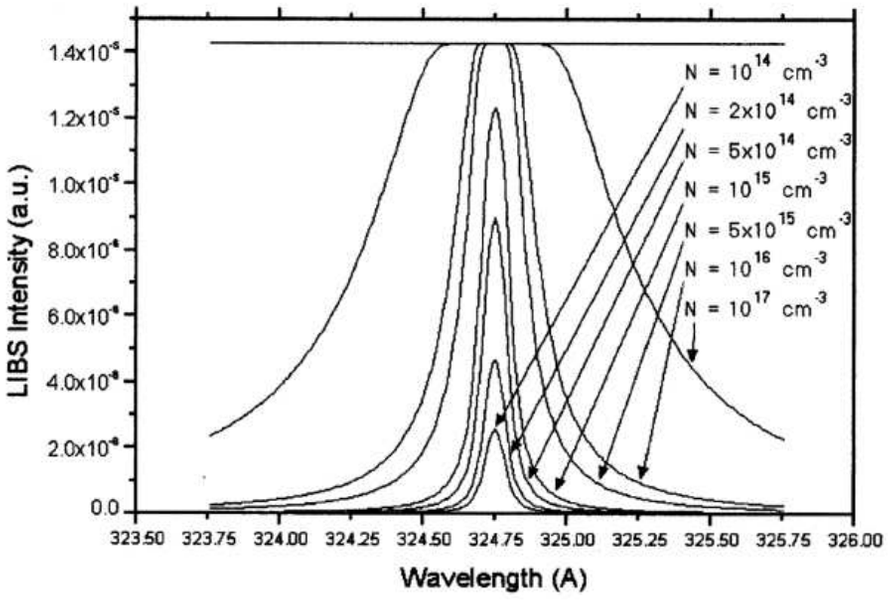

Figure 6. Simulation of Cu spectral line profile at 324.7 nm at different degrees of self-absorption.

4.5. Internal reference method

Sun and Yu [17] introduced a simplified procedure for correction of self-absorption by calibration-free laser-induced breakdown spectroscopy technique (CF-IBS). They utilized an internal reference line for each species. Then, they made a comparison between this spectral line with the other line intensity from the same species of the reference line to evaluate the self-absorption magnitude of the other spectral lines.

They started their method, i.e. internal standard self-absorption correction (IRSAC) by assumption of the plasma being in LTE condition, they estimated the measured integral line intensity as below:

$$I_{\lambda}^{ij} = f_{\lambda}^{b} F C_s A_{ij} \frac{g_i}{Z_s(T)} e^{-E_i / k_B T}, \tag{33}$$

where, A_{ij}, K_B, C_s, g_i, and λ are the transition probability, Boltzmann constant, the total densities of the emitting species s, the degeneracy of upper level i and wavelength of the transition, respectively. f_{λ}^{b} is self-absorption coefficient (the same SA) at wavelength λ, which has a magnitude between 0 and 1. F is a constant which includes the optical efficiency of the collection system, the total density of plasma and its volume. $Z_s(T)$ is the partition function of the analyzed spectral line. Here, the transition parameters of g_i, A_{ij} and E_i are inserted from spectral databases, and the magnitudes of F, C_s and T are extracted from the experimental data. According to the calibration-free method, the concentration of all the elements in the sample can be calculated by

http://dx.doi.org/10.5772/61941

$$C_s = \frac{1}{F} U_s(T) e^{q_s}. \tag{34}$$

where, $q_s = \ln \frac{C_s F}{U_s(T)}$. The self-absorption coefficient can be estimated by considering the ratio of the other emission intensities to an internal reference line for each species as

$$\frac{f_\lambda^b}{f_{\lambda_R}^b} = \frac{I_\lambda^{ij}}{I_{\lambda_R}^{mn}} \frac{A_{mn} g_m}{A_{ij} g_i} e^{-E_m - E_i / k_B T}, \tag{35}$$

here, $I_{\lambda_R}^{mn}$, λ_R, and $f_{\lambda_R}^b$ are spectral line intensity, wavelength, and self-absorption coefficient, respectively, of the mentioned reference line. A_{mn}, E_m, and g_m are the transition parameters related to the atomic levels *m* and *n*. It is assumed that the internal reference line has negligible self-absorption so that $f_{\lambda_R}^b \approx 1$. Hence, the self-absorption coefficient of other spectral lines are calculated by the following equation:

$$f_\lambda^b = \frac{I_\lambda^{ij} A_{mn} g_m}{I_{\lambda_R}^{mn} A_{ij} g_i} e^{-E_m - E_i / k_B T}. \tag{36}$$

Finally, the corrected line intensities without any self-absorption can be evaluated from the signal ratio of the measured spectral line intensity to the self-absorption coefficient as

$$\hat{I}_\lambda^{ij} = \frac{I_\lambda^{ij}}{f_\lambda^b} = \frac{I_{\lambda_R}^{mn} A_{ij} g_i}{A_{mn} g_m} e^{-E_m - E_i / k_B T}. \tag{37}$$

By utilizing Eq. (37), the self-absorption correction for each spectral line can be estimated. When these corrections are inserted to every point in the Boltzmann plot, the scattering of the points from each species around the best fit line will be decreased, and then more accurate quantitative results will be attained.

The outline of the IRSAC model is shown in this reference. Based on Eq. (36), for estimation of self-absorption coefficients, the plasma temperature must be known, which is initially calculated from Boltzmann plot curve without requiring any correction. The corrected line intensities by the previous temperature are utilized for evaluation of a new temperature. Since the magnitude of self-absorption straightly depends on the plasma temperature, the optimal self-absorption coefficients can be calculated by an iterative procedure up to attain a convergence in the correlation coefficients on the Boltzmann plot. After convergence of the correlation coefficients, the corrected points will be placed approximately on parallel linear Boltzmann

plot and the calculated temperatures from two successive iterations will alter a little. For more illustrations, a schematic of the Boltzmann plot for neutral atoms and singly ionized element is shown in Figure 7 before correction by the basic CF-LIBS method and IRSAC model.

In this experiment, a Q-switched Nd:YAG laser with pulse duration of 10 ns, laser energy of 200 mJ, wavelength of 1064 nm, and repetition rate of 1–15 Hz is focused on an aluminum alloy sample. For this sample, the acquisition delay time and integration gate width are adjusted for 2.5 μs and 1 ms, respectively.

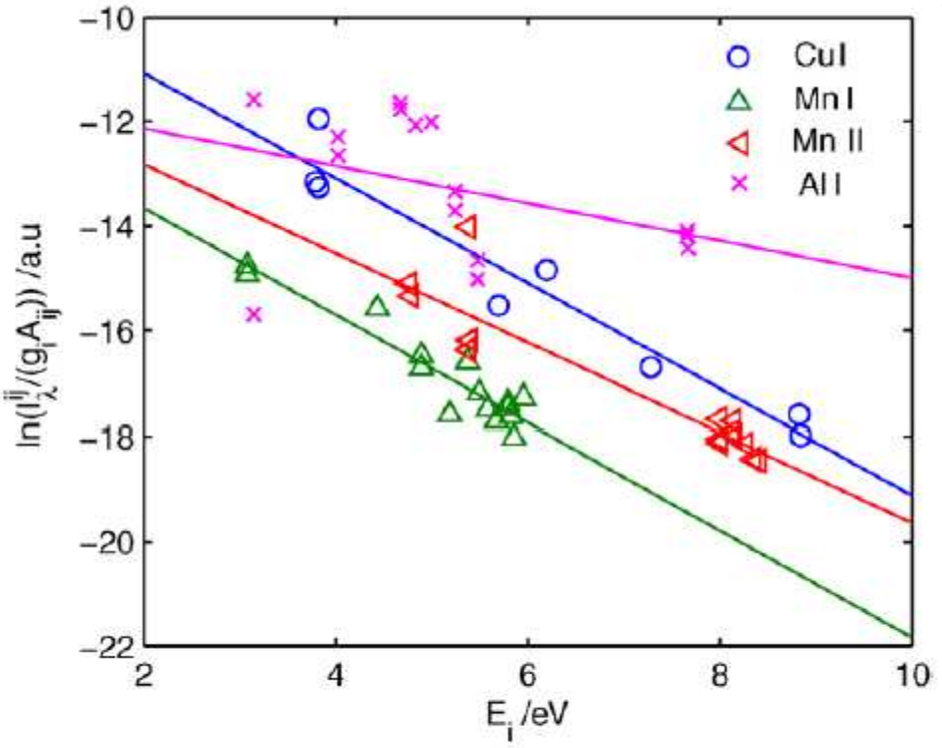

Figure 7. Initial Boltzmann plot which is depicted from spectral intensities of the alloys of aluminium samples.

4.6. Duplicating mirror

Moon et al. [8] duplicated the emission from a plasma by putting a spherical mirror at twice the distance of its focal length from the plasma. They evaluated the existence of optically thick plasma conditions by a very quick check-up. They acquired two line profiles (with and without applying the mirror) for determination of the amount of self-absorption in order to correct the spectral lines.

By taking into account the theoretical consideration, they evaluated the emission from a spatially homogeneous plasma distribution by the presence and absence of a mirror as below:

$$B_{\lambda,1} = B_{\lambda}^{bb}(1 - \exp[-k_{\lambda} l]). \tag{38}$$

$$B_{\lambda,2} = B_{\lambda,1} + GB_{\lambda,1}\exp(-k_\lambda l) = B_{\lambda,1}\left[1 + G\exp(-k_\lambda l)\right]. \quad (39)$$

In the above equation, the indexes 1 and 2 refer to the measurements with and without inserting the mirror, respectively. B_λ^{bb} indicates the spectral radiance of black body emission by the Wien or the Planck laws. In this calculation, G comprises both reflection and absorption losses of the mirror and in addition, solid angles produce imperfect matching. *G* can be computed by taking the ratio of signal intensity of continuous radiation, where $k_\lambda = 0$, i.e. at the line wings with negligible absorption as

$$R^c = \frac{B^c_{\lambda,2}}{B^c_{\lambda,1}} = 1 + G. \quad (40)$$

Furthermore, the ratio of peak intensities with and without considering mirror can be expressed as

$$R_\lambda = \frac{B_{\lambda,2}}{B_{\lambda,1}} = 1 + G\exp(-k_\lambda l). \quad (41)$$

The optical depth variations can also be evaluated by knowing the parameters of R^c and R_λ as:

$$\tau = k_\lambda l = \ln\frac{\left[R^c - 1\right]}{\left[R_\lambda - 1\right]}. \quad (42)$$

Finally, the correction factor $K_{\lambda,corr}$ (which is the inverse of the self-absorption coefficient SA) can be calculated experimentally versus the ratios of R^C and R^λ as:

$$K_{\lambda,corr} = \ln\frac{\left[(R^c - 1)/(R_\lambda - 1)\right]}{1 - \dfrac{(R_\lambda - 1)}{(R^c - 1)}}. \quad (43)$$

Furthermore, the duplication factor can be calculated from the following equation as

$$D_\lambda(\lambda) = \frac{B_\lambda(\lambda, 2fn_a l) - B_\lambda(\lambda, fn_a l)}{B_\lambda(\lambda, fn_a l)}, \quad (44)$$

where, $D_\lambda(\lambda)$ illustrates the relative growth in spectral line intensity or integral absorption created by doubling the value of ($fn_a l$) with two asymptotic magnitudes of 1 (at low optical

depths) and 0.415 (at high optical depths). Here, f, n_a and l refer to oscillation strength, number density, and plasma length, respectively. In this work, the plasma emission is produced by irradiation of a Nd:YAG laser with 90 ± 5 mJ pulse energy, 1064 nm laser wavelength, 6 ns pulse duration, and 1 Hz repetition frequency on the sample surface. The ICCD is adjusted for a delay time of 1 μs. Figure 8 expresses the results for analysis of Cu spectral line at 510.55 nm. Figures 8(a) and 8(b) show the evolution of R_λ and $K_{\lambda,corr}$ as a function of wavelength. As it is seen in Figure 8(a), the peak of spectral line saturates faster rather than that in line wings by doubling the plasma length. For obtaining the exact value of the correction factor $K_{\lambda,corr}$, the ratio of R_λ is estimated pixel by pixel. Furthermore, Figure 9 illustrates the evolution of calculated self-absorption correction factor $K_{\lambda, corr}$ as a function of R_λ and R^c. As it is seen in this figure, for the experimental R^c data, and by approaching R_λ to unity, the spectral lines are severely self-absorbed by including high values for correction factor $K_{\lambda, corr}$.

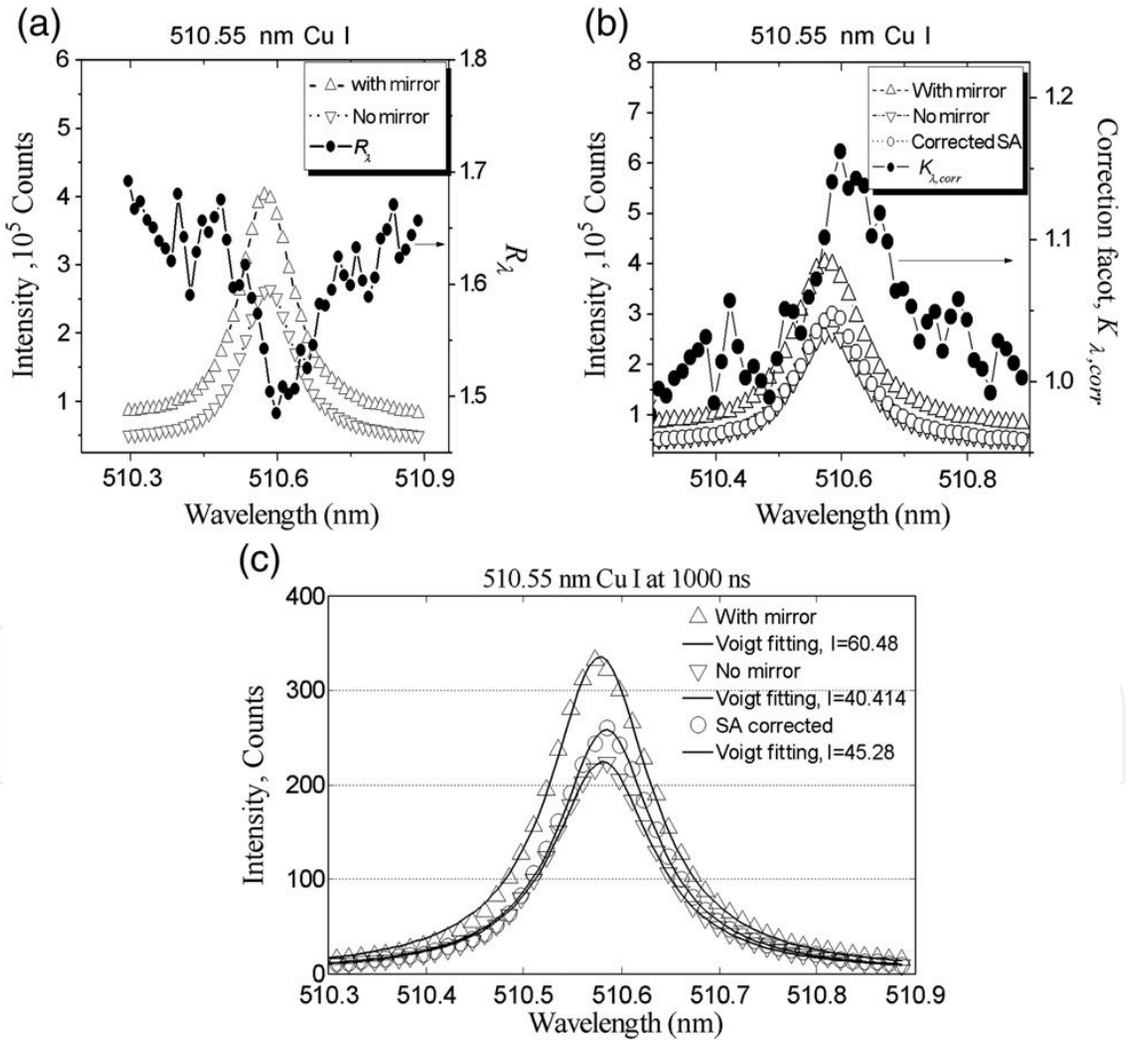

Figure 8. (a) Calculated data of R_λ versus wavelength, (b) evolution of correction factor $K_{\lambda,corr}$ versus line profiles corrected by self-absorption effect and wavelength. All curves are related to the spectral line Cu I at 510.55 nm, and at 1.0 μs delay time.

http://dx.doi.org/10.5772/61941

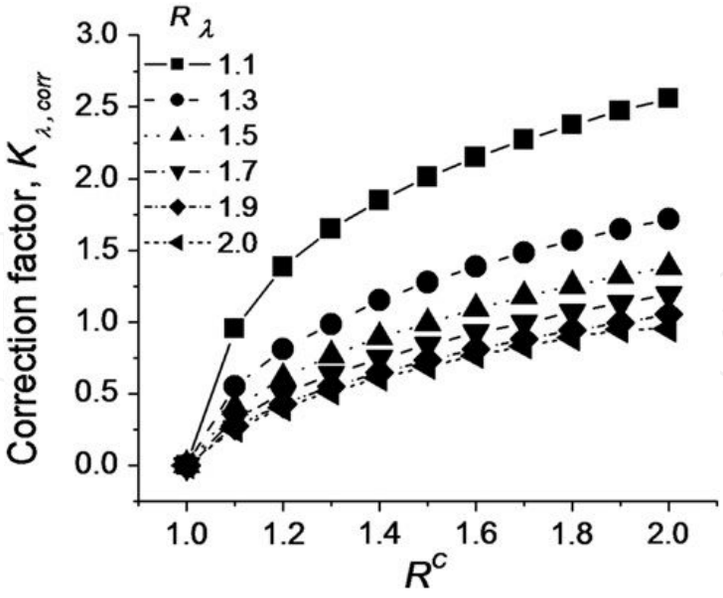

Figure 9. The dependence of the calculated correction factor $K_{\lambda,corr}$ to R_C, for different amounts of R_λ, or different levels of self-absorption.

4.7. Three lines method

Rezaei and Tavassoli [18] introduced the three lines method for studying optically thick plasma in local thermodynamic equilibrium by LIBS method without needing any spectral correction. They performed a LIBS experiment on an aluminum target in air atmosphere by utilizing the two techniques of spectroscopy and shadowgraphy, as well as by applying a theoretical approach.

In this study, plasma parameters were accurately determined by obtaining the plasma length, electron density, and intensities of three spectral lines from experiments. The model explains that instead of utilizing two spectral lines in thin plasmas, three lines are needed in thick plasmas for accurate evaluation of plasma temperature.

The thick plasma emission per unit volume, per unit time, and per unit frequency can be evaluated by replacing the multiplication of self-absorption coefficient by thin plasma intensity as:

$$I_{thick} = SA \times I_{thin} = \frac{(1-e^{-kl})}{(1-e^{-\frac{hc}{\lambda_0}\frac{1}{k_B T}})} \frac{C8\pi}{\lambda_0^2} e^{-\frac{(E_u - E_l)}{k_B T}} (\mathrm{SI}). \tag{45}$$

The parameters inserted in the above equation were introduced in previously mentioned equations. Here, Z is the partition function, which is computed by two and three level methods [29]. C is instrumental function which includes the efficiency and the solid angle of the detection system [30]. Here, k (m^{-1}) is the absorption coefficient which contains both contri-

bution of the stimulated emission of upper level and the absorption of lower level in the SI units such as in the following equation:

$$k = \frac{g_u A_{ul} N_{Al} \lambda_0^2}{8\pi Z} e^{-\frac{E_l}{k_B T}} (1 - e^{-\frac{h\nu_0}{k_B T}}) L(\nu, \nu_0, \gamma_{ul}). \tag{46}$$

$L(\nu, \nu_0, \gamma_{ul})$ is the Lorentzian line profile because of Stark broadening mechanism. γ_{ul} is the decay rate with a straight dependence to the line width as below [31]:

$$\gamma_{ul} = 2\pi(c / \lambda_0^2)\Delta\lambda_{stark}. \tag{47}$$

$\Delta\lambda_{stark}$ is full-width at half-maximum (FWHM) of the spectral line, which is produced due to Stark effect and is defined as follows [32]:

$$\Delta\lambda_{stark} = \frac{2\omega n_e}{n_{ref}}, \tag{48}$$

here, ω and n_e are electron impact parameter and electron number density, respectively. n_{ref} is the reference electron density (here, 10^{16} cm^{-3}) in which ω is calculated.

As mentioned in Eq. (45), for the spatially integrated plasma emission, the ratio of selected spectral lines can be written as below:

$$\frac{I_{thick\_1}}{I_{thick\_2}} - \frac{(1 - e^{-k_1 l})}{(1 - e^{-k_2 l})} \times \frac{(1 - e^{-\frac{hc}{\lambda_{02}}\frac{1}{k_B T}})}{(1 - e^{-\frac{hc}{\lambda_{01}}\frac{1}{k_B T}})} \times \frac{\lambda_{02}^2}{\lambda_{01}^2} \times \frac{e^{\frac{1}{k_B T}(E_{l1} - E_{u1})}}{e^{\frac{1}{k_B T}(E_{l2} - E_{u2})}} = 0. \tag{49}$$

$$\frac{I_{thick\_2}}{I_{thick\_3}} - \frac{(1 - e^{-k_2 l})}{(1 - e^{-k_3 l})} \times \frac{(1 - e^{-\frac{hc}{\lambda_{03}}\frac{1}{k_B T}})}{(1 - e^{-\frac{hc}{\lambda_{02}}\frac{1}{k_B T}})} \times \frac{\lambda_{03}^2}{\lambda_{02}^2} \times \frac{e^{\frac{1}{k_B T}(E_{l2} - E_{u2})}}{e^{\frac{1}{k_B T}(E_{l3} - E_{u3})}} = 0. \tag{50}$$

It should be noted that both of the above equations satisfy at particular T and N_{Al}. Consequently, the cross of two equations (i.e. left-hand side of equations) with the contour of zero (i.e. right-hand side of equations) is the answer. Therefore, by depicting the contour plot of the above equations and crossing them, the passive parameters of T and N_{Al} is gotten at a particular delay time and at specific laser energy. Then, by inserting these data (answer) in one of the above equations, the instrumental function C will be obtained.

4.8. Line ratio analysis

Bredice et al. [33] utilized the theoretical treatment companioned by experimental results for estimation of the amount of self-absorption in single and collinear double pulse configuration. They used the two-line ratio analysis of the same species of manganese element in Fe–Mn alloys to characterize the homogenous plasma parameters. Moreover, they calculated the self-absorption coefficient by considering the line ratios in different conditions: two lines reveal weak or no self-absorption, two lines experience strong self-absorption, two lines belong to the same multiplet, and two lines are general cases as well. Their results are summarized as the following:

1. Limit case: two negligible self-absorbed lines:

When two lines are weakly self-absorbed, i.e. $(SA)_1=(SA)_2=1$ (or $\kappa_{1,2}(\lambda_0)l<<1$), the ratio of the two spectral intensities from the similar species can be expressed as

$$\frac{(N_p)_2}{(N_p)_1} \approx \frac{(A_{ki}g_k e^{-\frac{E_k}{k_B T}})_2}{(A_{ki}g_k e^{-\frac{E_k}{k_B T}})_1}. \qquad \kappa_{1,2}(\lambda_0)l << 1 \tag{51}$$

It should be noted that in this calculation, N_p indicates the integral intensity of the selected spectral line and also, other parameters are introduced before.

2. Limit case: severely self-absorbed spectral lines:

When two spectral lines are exposed to strong self-absorption, the self-absorption coefficients can be calculated as:

$$SA \approx \frac{1}{\kappa(\lambda_0)l}. \tag{52}$$

Therefore, the spectral ratios of spectral emissions of the same species, both exposed to strong self-absorption, can be calculated by

$$\frac{(N_p)_2}{(N_p)_1} \approx \left[\frac{(A_{ki}g_k e^{-\frac{E_k}{k_B T}})_2}{(A_{ki}g_k e^{-\frac{E_k}{k_B T}})_1}\right] \left[\frac{\left(\frac{\lambda_0^4 A_{ki}g_k e^{-\frac{E_i}{k_B T}}}{\Delta\lambda_0}\right)_1}{\left(\frac{\lambda_0^4 A_{ki}g_k e^{-\frac{E_i}{k_B T}}}{\Delta\lambda_0}\right)_2}\right]^{\beta} \qquad \kappa_{1,2}(\lambda_0)l >> 1 \tag{53}$$

3. Limit case: two lines related to the same multiplet

In two spectral lines belonging to the same multiplet, the atomic energies of E_i and E_k are similar and it is obtain an intensity ratio that is constant with plasma temperature variation. In this regime, by considering the above situations, the intensity ratio can be located between the two extremes as

$$\frac{(N_p)_2}{(N_p)_1} = \left[\frac{(A_{ki}g_k)_2}{(A_{ki}g_k)_1}\right]^{(1-\beta)} \left[\frac{(\lambda_0^4)_1}{(\lambda_0^4)_2}\right]^{\beta} \qquad \kappa_{1,2}(\lambda_0)l >> 1, \tag{54}$$

$$\frac{(N_p)_2}{(N_p)_1} \approx \frac{(A_{ki}g_k)_2}{(A_{ki}g_k)_1} \qquad \kappa_{1,2}(\lambda_0)l << 1 \tag{55}$$

in the case of high and low self-absorption, respectively.

4. General case

For two arbitrary spectral lines, the spectral intensities ratios can be evaluated by

$$\begin{aligned}\frac{(N_p)_2}{(N_p)_1} &= \frac{(A_{ki}g_k e^{-\frac{E_k}{k_B T}})_2}{(A_{ki}g_k e^{-\frac{E_k}{k_B T}})_1} \left(\frac{k(\lambda_0)_1}{k(\lambda_0)_2} \frac{(1-e^{-k(\lambda_0)_2 l})}{(1-e^{-k(\lambda_0)_1 l})}\right)^{\beta} \\ &= a\left[\frac{b(1-e^{-k(\lambda_0)_2 l})}{(1-e^{bk(\lambda_0)_2 l})}\right]^{\beta}.\end{aligned} \tag{56}$$

$$\begin{aligned} a &= \frac{(A_{ki}g_k e^{-\frac{E_k}{k_B T}})_2}{(A_{ki}g_k e^{-\frac{E_k}{k_B T}})_1}, \\ b &= \frac{(\lambda_0^4 A_{ki}g_k e^{-\frac{E_i}{k_B T}})_1}{(\lambda_0^4 A_{ki}g_k e^{-\frac{E_i}{k_B T}})_2} \left(\frac{(\Delta\lambda_0)_2}{(\Delta\lambda_0)_1}\right). \end{aligned} \tag{57}$$

In order to find numerically $k(\lambda_0)_2 l$, the intensity ratio of two spectral lines $\frac{(N_p)_2}{(N_p)_1}$, the line broadening ratio $\frac{(\Delta\lambda_0)_2}{(\Delta\lambda_0)_1}$, and plasma temperature T must be determined from the experiment.

By knowing the $k(\lambda_0)l$ for a spectral line, the self-absorption coefficient SA can be carefully calculated.

For instance, in order to show the application of the mentioned theoretical equations, Figure 10 is depicted. In this experiment, Nd-YAG laser pulses at 1064 nm with 7 and 12 ns FWHM and various laser energies are irradiated on Fe-Mn alloys. The experiment is performed at different places in single and double pulse configurations. Figure 10 illustrates the signal ratios of the spectral lines of Mn II at 293.3 to Mn II at 294.9 nm (lines related to the same multiplet) and ratio of Mn II at 293.3 to spectral line of Mn II at 348.3 nm (lines belong to different multiplets) as a function of delay time. Temporal evolution of intensity ratio is plotted as a function of the acquisition delay time in two situations of single and double pulse measurements. In double pulse measurements, the delay time is considered after the arrival of the second pulse on the sample. Since the first two lines, i.e. Mn II lines at 293.3 and 294.9 nm, belong to the similar multiplet, the theoretically mentioned equation is applicable. As shown in the theory, if two limit cases of low or high self-absorption are satisfied, the intensity ratio of these two lines will be particularly independent of the plasma variation.

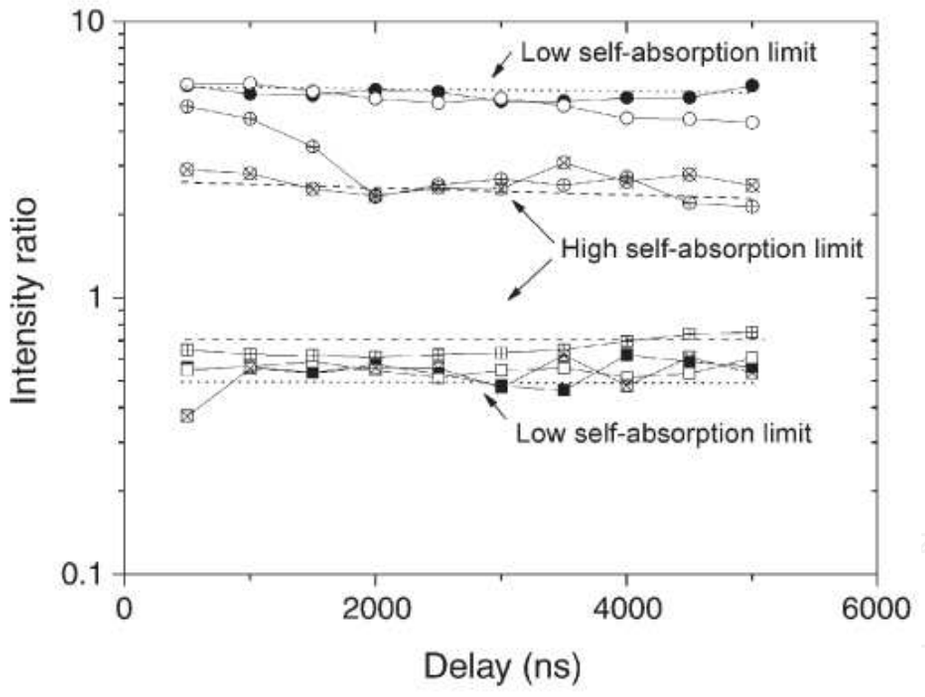

Figure 10. Temporal evolution of intensity ratios of of two spectral lines of Mn II at 293.3 and Mn II at 294.9 nm (full squares, laser energy of 60 mJ, open squares, 120 mJ and crossed squares, 200 mJ laser energy, diagonally crossed squares, 60 + 60 mJ double pulse irradiation) and for Mn II at 293.3/Mn II at 348.3 nm lines (full circles, 60 mJ laser energy, open circles, 120 mJ laser energy, crossed circles, 200 mJ laser energy, diagonally crossed circles, 60 + 60 mJ double pulse measurements).

It should be noted that the dotted line shows the limit of low self-absorption and dashed line indicates the high self-absorption limits. Furthermore, in both lines, y axis is in logarithmic scale. Cristoforetti and Tognoni [19] calculated the concentration ratio of different elements by

assumption of holding a homogeneity condition in plasma without needing any self-absorption correction. Furthermore, by obtaining the columnar densities, they computed the plasma temperature and the number densities of different plasma species.

In this work, first, by numerical calculation of the optical depth $k(\lambda_0)l$, the SA parameter is computed by exploiting Eq. (16), as shown in Figure 11. After that, the columnar density n_{il} can be easily extracted by rewriting the equation of optical depth as

$$\left(n_i l\right)_{17} = 1770 \frac{\Delta\lambda_0}{f\lambda_0^2} k(\lambda_0) l, \tag{58}$$

here, $\Delta\lambda_0$ is the expected line width in the case of thin plasma, $(n_{il})_{17}$ is explained in 10^{17} cm^{-2} units, and λ_0 and $\Delta\lambda_0$ are written in Angstrom units. By knowing the columnar density, the inverse of plasma temperature can be calculated from the slope of the line obtained by fitting the points in the Saha–Boltzmann plot.

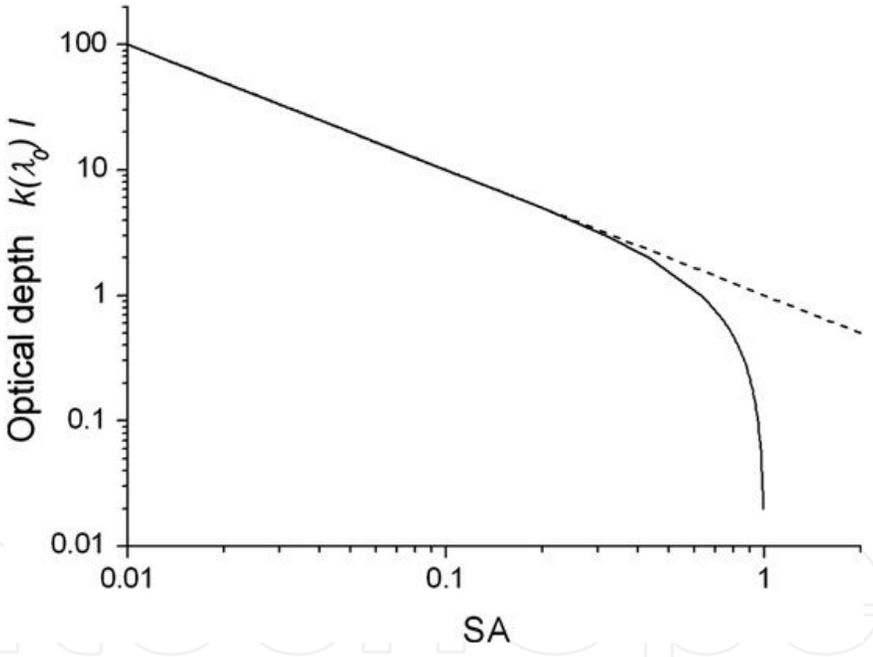

Figure 11. Relation between optical depth and the SA coefficient.

5. Inhomogeneous plasma

Different schematics of nonhomogeneous plasmas including 2, 5, *N*, and 250 sections in cylindrical and spherical shapes are investigated for thick plasma analysis by considering self-absorption correction as in the figures below:

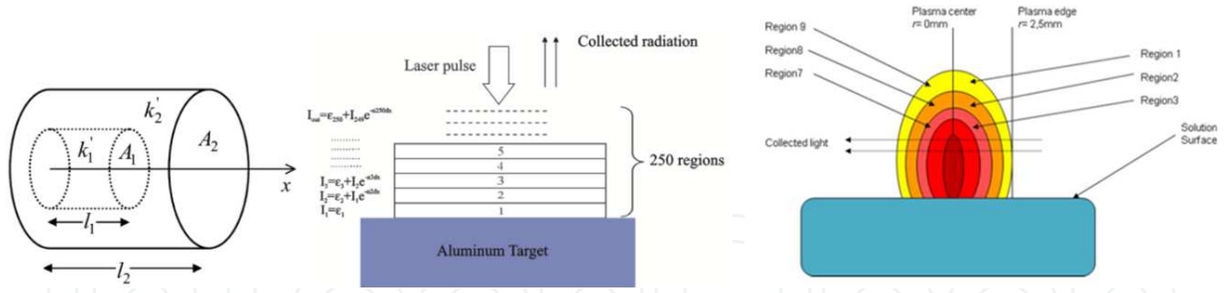

Figure 12. Different schematics of nonhomogeneous thick plasmas [10, 13, 34].

The methods of all of above schematics are approximately similar, so that all of them utilize the emission of internal layers plus attenuation from outer regions. Therefore, the calculations related to 250 layers as well as another numerical model including *N* layer are explained in the following section.

Rezaei et al. [34] studied the spectral emissions of an aluminum sample located in argon and helium noble gases at 1 atm pressure, by applying a numerical calculation. They computed the plasma parameters by coupling the thermal model of laser ablation, hydrodynamic of plasma expansion, and Saha–Eggert equations. In that model, the spectral emissions were constructed from the superposition of some strong lines of aluminum and several strong lines of ambient gases, which were superimposed on a continuous radiation composed of brems-strahlung and recombination emissions. Moreover, they calculated the spectral emissions in two cases of thin and thick plasmas by considering the self-absorption influence.

In this work, the plasma is supposed to be consisted of 250 layers with 60-μm thickness (as shown in Figure 12). Each section of this plasma is characterized by specific plasma parameters, such as temperature, electron density, mass densities, and number densities of plasma species as a function of delay time. The plasma radiations of different layers are collected in a parallel direction to the laser pulse. The emission of the first layer quite above the sample surface due to its own radiation can be expressed by:

$$I_{(1)} = \varepsilon_{spec(1)} = \sum_{j=1}^{N_s} N_u^{(1)} A_{ul}^j h\nu_j L_j^{(1)}(\nu, \nu_j, \gamma_{ul}^j). \tag{59}$$

The contribution of the second layer toward the optical collecting system, which comprises both of its radiation and attenuation of the first layer is calculated from:

$$I_{(2)} = \sum_{j=1}^{N_s} N_j^{(2)} A_{ul}^j h\nu_j L_j^{(2)}(\nu\ , \nu_j, \gamma_{ul}^j) + \varepsilon_{spec(1)} e^{-k_{(2)}dx} = \varepsilon_{spec(2)} + I_{(1)} e^{-k_{(2)}dx}. \tag{60}$$

Consequently, the spectral intensity of the nth layer due to the whole sequential absorption is defined as:

$$I_{(n)} = \sum_{j=1}^{N_s} N_j^{(n)} A_{ul}^j h\nu_j L_j^{(n)}(\nu\ ,\nu_j,\gamma_{ul}^j) + I_{(n-1)} e^{-k_{(n)}dx} = \varepsilon_{spec(n)} + I_{(n-1)} e^{-k_{(n)}dx}. \quad (61)$$

According to the two-level system, the absorption coefficient is expressed by inserting the contributions of the absorption and induced emission between the levels of u and l as

$$k_{(n)} = \frac{h\nu_j}{c}(B_{ul}N_l - B_{lu}N_u)L^{(n)}{}_j(\nu,\nu_j,\gamma_{ul}^j)\big(\mathrm{SI}\big), \quad (62)$$

Here, B_{ul} and B_{lu} are Einstein coefficients related to the absorption and induced emission (m^3J s), respectively. Finally, the self-absorbed spectral intensity is the emission of last layer (i.e 250^{th} layer) which includes the entire regions shown below for attenuation as follows:

$$I_{selfabsorb} = \varepsilon_{(250)} + I_{(249)} e^{-k_{(250)}dx}. \quad (63)$$

For comparison between thick plasma emissions with a non-self-absorbed spectral line in a thin plasma condition, the summation over all strong line radiations, including the contribution of the whole layers, can be considered as

$$I_{nonselfabsorb}(\nu,\nu_j) = \sum_{k=1}^{k_s}\sum_{j=1}^{Ns} \varepsilon_{spec}^j(\nu,\nu_j), \quad (64)$$

where, k_s and N_s are the number of plasma layers and the number of strong lines, respectively. For instance, the effect of pulse laser energy on Al spectral lines at 394.40 and 396.15 nm is shown in Figure 13 in the logarithmic scale. Here, a Gaussian-shaped laser pulse, with a wavelength of 266 nm, FWHM of 10 ns, under different laser irradiances is focused on aluminum sample. As it is seen by increasing laser intensities, the self-absorption coefficient grows. The magnitudes of self-absorption coefficients in two ambient gases of Ar and He are inserted in this reference.

Furthermore, Ben Ahmed and Cowpe proposed a nonhomogeneous plasma with five layers as shown in Figure 12, and, then, they calculated the total observed intensity by taking into account the *i* and *j* regions as:

$$I = \sum_i \left(\frac{I_i}{\tau_i}(1 - exp(-\tau_i))exp(\sum_{j>i}(-\tau_j)) \right). \quad (65)$$

Lazic et al. [16] considered a cylinder with length L including homogenous density and temperature, which is divided into N similar thin layers with length δL surrounded by another

http://dx.doi.org/10.5772/61941

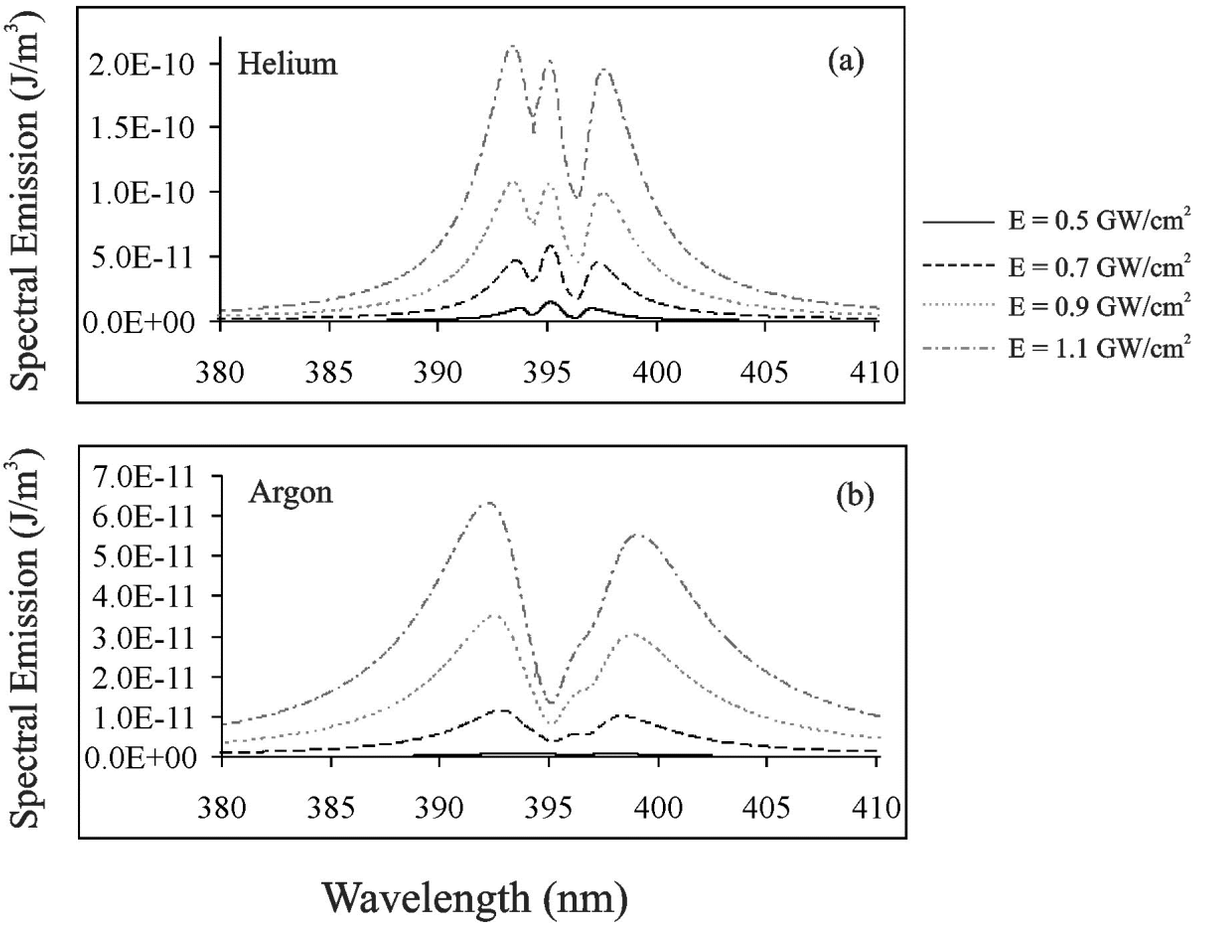

Figure 13. Self-reversal evolutions of the spectral lines of 394.40 and 396.15 nm, at different laser energies of 0.5, 0.7, 0.9, and 1.1 GW/cm^2 in (a) helium and (b) argon gas.

outer thin layer. Similar to the above-mentioned method, by considering successive absorption and using the seri summation result, they expressed the total line intensity escaping from plasma as

$$I_{\alpha}^{ki} = FC_{\alpha}\frac{f_{\alpha}^{ki}(T)}{U_{\alpha}(T)}\frac{1-e^{-\beta^{ik}C_{\alpha}^{i}L}}{L/\delta L\left(1-e^{-\beta^{ik}C_{\alpha}^{i}\delta L}\right)}. \tag{66}$$

where, C_{α} is the total species concentration and C_{α}^{i} is the concentration of species at lower level i which is related to the C_{α} by Boltzmann equation. f_{α}^{ki} comprises the all parameters correspond to ki transition. $U_{\alpha}(T)$ is partition function and F is a constant attributed to the experimental condition. Then, by assumption of existence of a thin colder plasma surrounding the cylindrical plasma, the overall emission is obtained as below:

$$I_\alpha^{ki} = F_1 C_\alpha \frac{f_\alpha^{ki}(T)}{U_\alpha(T)} \times \frac{1 - e^{-\frac{\beta^{ik} H_\alpha^i C_\alpha L}{U_\alpha(T)}}}{L/\delta L \left(1 - e^{-\frac{\beta^{ik} H_\alpha^i C_\alpha \delta L}{U_\alpha(T)}}\right)} + F_2 C_\alpha \frac{f_\alpha^{ki}(T)}{U_\alpha(T)}. \tag{67}$$

where, $H_\alpha^i = g_i e^{-\frac{E_i}{K_B T}}$. F_1 and F_2 are constants related to optically thick and thin plasma, respectively, and are straightly dependent on the plasma geometry.

By combination of the above equations, a relation is obtained which connect the raw measured element concentration C_m to effective element concentration C_E as follow:

$$C_m = \frac{a_1}{a_2}\left(1 - e^{-a_2 C_E}\right) + a_3 C_E. \tag{68}$$

The first term in the above equation is attributed to the optically thick plasma and a_i are coefficients that can be determined by fitting to the experimental results. Figure 14 illustrates the measured spectral emission of Cu at 327.39 nm versus certified concentration for different selected samples. In this experiment, a third harmonic Nd:YAG pulsed laser beam with energies of 6–10 mJ is focused on soil and sediment samples. The acquisition delay time is adjusted for 300 ns and the gate width is 1000 ns for all examined samples.

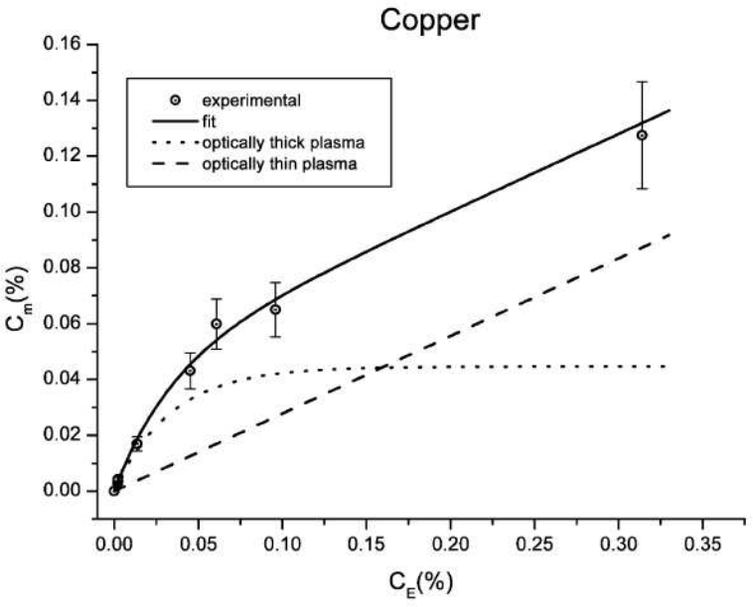

Figure 14. Measured LIBS emission for Cu spectral line at 327.39 nm as a function of certified concentrations.

Some research groups used self-absorbed spectral lines for charactrizing the plasma properties by proposing appropriate models without needing to any self-absorption correction as

mentioned in Section (7. IV). In addition, Gornushkin et al. [35] introduced a semiempirical model for an optically thick inhomogeneous plasma in LTE condition. In this model, the input parameters are the ratio of atomic species and plasma pressure or the number of plasma elements, which were all measured from the experiments. Some functions are introduced for calculation of plasma temperature and its size variation. The outputs of this model are time and space evolutions of species number densities, variations of optical depth and spectral line profiles, as well as the resulting intensity of spectral emission close to the transition of strong nonresonance atomic line. The main application of this model is the prediction of electron density, temperature, and the mechanism of line broadening.

According to this model, the relation of the observed spectral radiance I_υ(erg.s^{-1}.cm^{-2}.sr^{-1}.Hz^{-1}) with absorption coefficient κ(ν, x, T) and distribution of volume emission coefficient ε_ν(ν, x, T) in optically thick plasma can be expressed by radiation transfer equation as

$$I_\nu = \int_{-x_0}^{x_0} \varepsilon_\nu(\nu, x, T) e^{-\tau(\nu, x, T)} dx. \tag{69}$$

τ(ν, x, T) is the plasma optical thickness which is expressed by:

$$\tau(\nu, x, T) = \int_{-x}^{x_0} \kappa(\nu, x, T) dx. \tag{70}$$

x_o and $-x_o$ refer to the plasma dimension from edge to edge along the line of sight. The magnitudes of volume emission ε_ν(ν, x, T) and the absorption κ(ν, x, T) coefficients in an inhomogenous plasma are not constant and vary with the position along the line of sight. Bartels and Zwicker [4, 5] proved that in the absence of stimulated transitions, Eq. (69) can be expressed as the multiplication of the below three terms as:

$$I_\nu = A(T_m).M(E_l, E_u).Y\left[\tau(\nu, x, T), p\right]. \tag{71}$$

The first term, A(T_m) is assumed as a source function which is related only to T_m and is the exact explanation for Wien's law:

$$A = \frac{2h\nu^3}{c^2} \exp\left(-\frac{h\nu}{kT_m}\right). \tag{72}$$

It should be noted that Omenetto et al. [36] expressed that the source function in Wien's law can be applied for plasmas in which stimulated transitions are not important and the condition of $h\nu/kT_m \gg 1$ holds, while Planck's law is utilized when stimulated transitions are taken into account.

The second term in Eq. (71) considers, to some extent, the influences of plasma heterogeneity on radiation and for spectral line with naturally and van der Waals broadening equals to:

$$M = \sqrt{\frac{E_l}{E_u}}. \qquad if \qquad \frac{kT_m}{E_l} << 1. \tag{73}$$

For singly ionized atoms and for neutral lines with Stark broadened, M can be expressed as

$$M = \sqrt{\frac{E_l + 0.5x_0}{E_u + 0.5x_0}}. \qquad if \qquad \frac{kT_m}{E_l + 0.5x_0} << 1 \tag{74}$$

Here, E_l and E_u are the lower and upper levels excitation energies, respectively and x_0 is the ionization energy. Furthermore, the above mentioned conditional statements in Eqs. (84) and (85) are not satisfied for resonance neutral lines, but they are logical assumptions for ionic spectral lines as well as for nonresonance neutral lines.

The third term in Eq. (71) considers the influences of heterogeneous mixing and optical thickness. The function $Y[\tau(\nu, x, T), p]$ is approximated by the below equation:

$$\begin{aligned} Y\left[\tau(\nu,x,T),p\right] &= e^{-\frac{\tau(\nu,x,T)}{2}}\left[\frac{\tau(\nu,x,T)}{2}(1-p)\right. \\ &+ p\sinh\left(\frac{\tau(\nu,x,T)}{2}\right) \\ &\left.+ \frac{1}{\sqrt{p}}\sinh\left(\frac{\tau(\nu,x,T)}{2}\sqrt{p}\right)\right]. \end{aligned} \tag{75}$$

Here, the parameter p is explained as

$$p = \frac{6}{\pi} arctg \frac{M^2}{\sqrt{1+M^2}}. \tag{76}$$

Therefore, by substitution of above equations into Eq. (71), spectral emission intensity for optically thick inhomogenous plasma I_υ can be obtained. In this model, the spatial distribution of plasma temperature is approximated by a second-order polynomial function with a maximum value in the plasma center.

Figure 15 represents the calculated emission distributions for different initial number of atoms and various Si/N atom ratios obtained at several distinct delay times (from 1 to 4 a.u.). In this figure, it is seen that at low densities (10^{16}), the plasma continuous emission (curves at t_1, t_2),

monotonically reduces by time passing and growing the plasma. In addition, at high densities (10^{17}), a considerable value of early plasma continuum is absorbed within the plasma plume, which causes less emission radiation at time t_1 compared to times t_2 and t_3. This results in the LIP to approach a black body emitter at initial delay times.

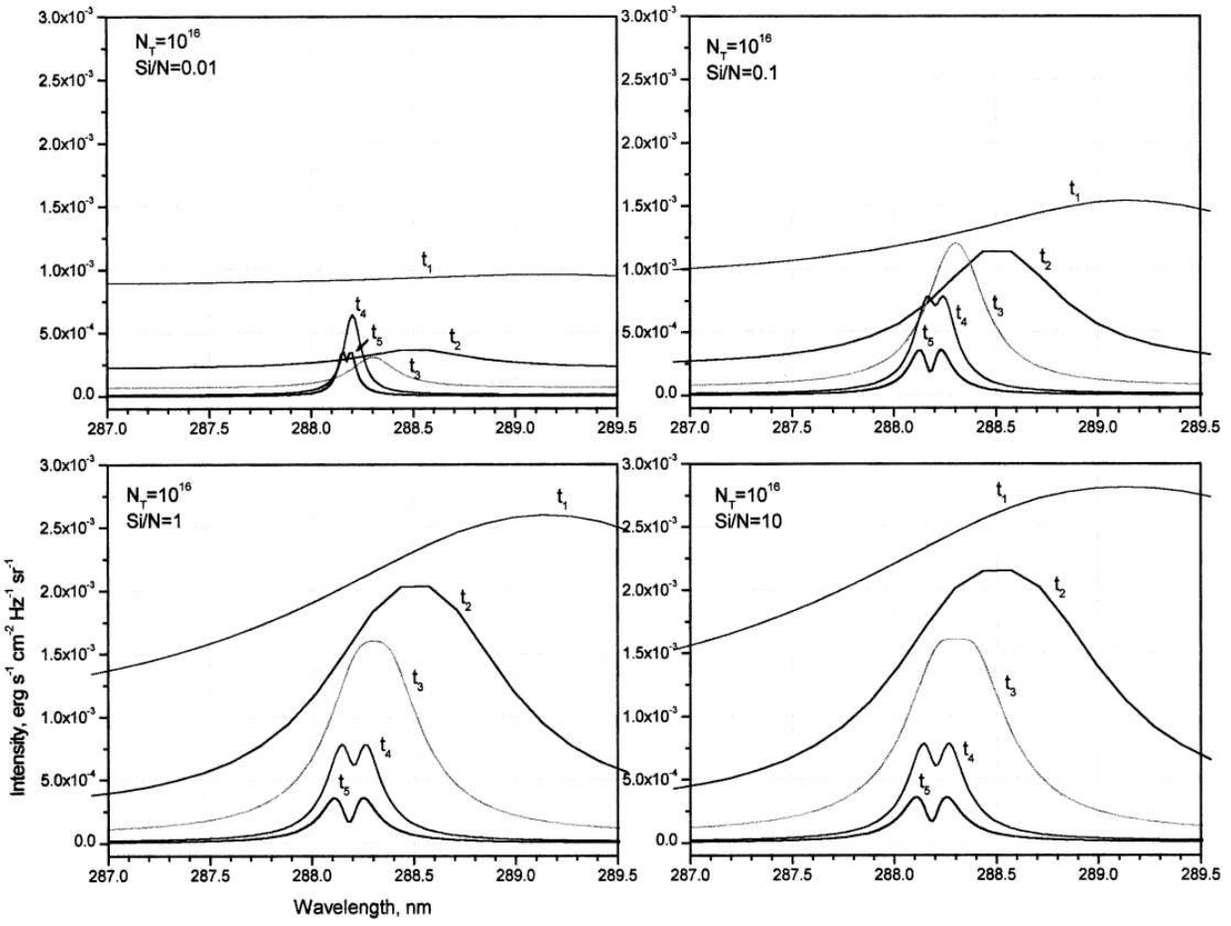

Figure 15. Calculated radiation profiles for LIP in initial times, including different proportions of 10^{16} N and Si atoms: from Si/N = 0.01 to Si/N =10. Times t_1 to t_5 refers to the magnitudes of 1, 1.5, 2, 3, and 4 in relative units.

Moreover, it must be mentioned that different research groups [37–41] discussed about spectrum analysis and extraction of plasma parameters in symmetric and asymmetric self-reversal line shapes produced by different sources that can be studied by readers for completeness of information.

6. Conclusion

In this chapter, a brief description of the different methods of analyzing the thick laser-produced plasmas was represented by considering the theoretical and experimental techniques. In some works, the self-absorption was corrected and then, the plasma parameters was

extracted, while in others, some proposed models were explained and thereafter, plasma features was obtained straightly without needing any correction.

Finally, it should be noted that different parameters such as laser features (its wavelength [42], double or single pulse scheme [33, 43], energy [34], and pulse duration [42]), ambient gas condition (the nature and its pressure [42, 44]) and measurement device circumstance (delay time [8, 34], gate width, and exposure time), and the sample characteristics (metal and biological cases) could affect the amount of self-absorption as well. The details of these effects can be studied in the related references.

Author details

Fatemeh Rezaei*

Address all correspondence to: fatemehrezaei@kntu.ac.ir

Department of Physics, K. N. Toosi University of Technology, Shariati, Tehran, Iran

References

[1] Ovsyannikov, A., *Plasma Diagnostics*. 2000: Cambridge Int Science Publishing.

[2] Aragón, C. and J. Aguilera, *CSigma graphs: A new approach for plasma characterization in laser-induced breakdown spectroscopy.* Journal of Quantitative Spectroscopy and Radiative Transfer, 2014. 149: p. 90–102.

[3] Cowan, R.D. and G.H. Dieke, *Self-absorption of spectrum lines.* Reviews of Modern Physics, 1948. 20(2): p. 418.

[4] Zwicker, H., *Evaluation of plasma parameters in optically thick plasmas.* Plasma Diagnostics, 1968.

[5] Bartels, H., *Z. Phys 125 597 Bartels H 1949.* Z. Phys, 1949. 126: p. 108.

[6] Amamou, H., et al., *Correction of self-absorption spectral line and ratios of transition probabilities for homogeneous and LTE plasma.* Journal of Quantitative Spectroscopy and Radiative Transfer, 2002. 75(6): p. 747–763.

[7] Amamou, H., et al., *Correction of the self-absorption for reversed spectral lines: application to two resonance lines of neutral aluminium.* Journal of Quantitative Spectroscopy and Radiative Transfer, 2003. 77(4): p. 365–372.

[8] Moon, H.-Y., et al., *On the usefulness of a duplicating mirror to evaluate self-absorption effects in laser induced breakdown spectroscopy.* Spectrochimica Acta Part B: Atomic Spectroscopy, 2009. 64(7): p. 702–713.

[9] Aguilera, J. and C. Aragón, *Characterization of laser-induced plasmas by emission spectroscopy with curve-of-growth measurements. Part I: Temporal evolution of plasma parameters and self-absorption.* Spectrochimica Acta Part B: Atomic Spectroscopy, 2008. 63(7): p. 784–792.

[10] Aguilera, J., J. Bengoechea, and C. Aragón, *Curves of growth of spectral lines emitted by a laser-induced plasma: influence of the temporal evolution and spatial inhomogeneity of the plasma.* Spectrochimica Acta Part B: Atomic Spectroscopy, 2003. 58(2): p. 221–237.

[11] Aragon, C., J. Bengoechea, and J. Aguilera, *Influence of the optical depth on spectral line emission from laser-induced plasmas.* Spectrochimica Acta Part B: Atomic Spectroscopy, 2001. 56(6): p. 619–628.

[12] Aragón, C., F. Peñalba, and J. Aguilera, *Curves of growth of neutral atom and ion lines emitted by a laser induced plasma.* Spectrochimica Acta Part B: Atomic Spectroscopy, 2005. 60(7): p. 879–887.

[13] Ben Ahmed, J. and J. Cowpe, *Experimental and theoretical investigation of a self-absorbed spectral line emitted from laser-induced plasmas.* Applied optics, 2010. 49(18): p. 3607–3612.

[14] Bulajic, D., et al., *A procedure for correcting self-absorption in calibration free-laser induced breakdown spectroscopy.* Spectrochimica Acta Part B: Atomic Spectroscopy, 2002. 57(2): p. 339–353.

[15] El Sherbini, A., et al., *Evaluation of self-absorption coefficients of aluminum emission lines in laser-induced breakdown spectroscopy measurements.* Spectrochimica Acta Part B: Atomic Spectroscopy, 2005. 60(12): p. 1573–1579.

[16] Lazic, V., et al., *Self-absorption model in quantitative laser induced breakdown spectroscopy measurements on soils and sediments.* Spectrochimica Acta Part B: Atomic Spectroscopy, 2001. 56(6): p. 807–820.

[17] Sun, L. and H. Yu, *Correction of self-absorption effect in calibration-free laser-induced breakdown spectroscopy by an internal reference method.* Talanta, 2009. 79(2): p. 388–395.

[18] Rezaei, F. and S.H. Tavassoli, *A new method for calculation of thick plasma parameters by combination of laser spectroscopy and shadowgraphy techniques.* Journal of Analytical Atomic Spectrometry, 2014. 29(12): p. 2371–2378.

[19] Cristoforetti, G. and E. Tognoni, *Calculation of elemental columnar density from self-absorbed lines in laser-induced breakdown spectroscopy: A resource for quantitative analysis.* Spectrochimica Acta Part B: Atomic Spectroscopy, 2013. 79: p. 63–71.

[20] Hermann, J., C. Boulmer-Leborgne, and D. Hong, *Diagnostics of the early phase of an ultraviolet laser induced plasma by spectral line analysis considering self-absorption.* Journal of applied physics, 1998. 83: p. 691–696.

[21] D'Angelo, C.A., D.M.D. Pace, and G. Bertuccelli, *Semiempirical model for analysis of inhomogeneous optically thick laser-induced plasmas.* Spectrochimica Acta Part B: Atomic Spectroscopy, 2009. 64(10): p. 999–1008.

[22] O'neill, R., *Algorithm AS 47: function minimization using a simplex procedure.* Applied Statistics, 1971: p. 338–345.

[23] Rezaei, F., P. Karimi, and S. Tavassoli, *Effect of self-absorption correction on LIBS measurements by calibration curve and artificial neural network.* Applied Physics B, 2014. 114(4): p. 591–600.

[24] Mitchell, A. and M.W. Zemansky, *Resonance Radiation*. 1934: Cambridge.

[25] Hinnov, E., *A method of determining optical cross sections.* JOSA, 1957. 47(2): p. 151–155.

[26] Alkemade, C.T.J., et al., *Th. Metal Vapours in Flames*. 1982, Pergamon Press: Oxford.

[27] Gornushkin, I., et al., *Curve of growth methodology applied to laser-induced plasma emission spectroscopy.* Spectrochimica Acta Part B: Atomic Spectroscopy, 1999. 54(3): p. 491–503.

[28] Demtröder, W., *Laser Spectroscopy: Basic Concepts and Instrumentation*. 2013: Springer Science & Business Media.

[29] D'Ammando, G., et al., *Computation of thermodynamic plasma properties: a simplified approach.* Spectrochimica Acta Part B: Atomic Spectroscopy, 2010. 65(8): p. 603–615.

[30] Aguilera, J. and C. Aragón, *Characterization of laser-induced plasmas by emission spectroscopy with curve-of-growth measurements. Part II: Effect of the focusing distance and the pulse energy.* Spectrochimica Acta Part B: Atomic Spectroscopy, 2008. 63(7): p. 793–799.

[31] Silfvast, W.T., *Laser Fundamentals*. 2004: Cambridge University Press.

[32] Griem, H.R., *Plasma Spectroscopy.* New York: McGraw-Hill, 1964, 1964. 1.

[33] Bredice, F., et al., *Evaluation of self-absorption of manganese emission lines in Laser Induced Breakdown Spectroscopy measurements.* Spectrochimica Acta Part B: Atomic Spectroscopy, 2006. 61(12): p. 1294–1303.

[34] Rezaei, F., P. Karimi, and S. Tavassoli, *Estimation of self-absorption effect on aluminum emission in the presence of different noble gases: comparison between thin and thick plasma emission.* Applied Optics, 2013. 52(21): p. 5088–5096.

[35] Gornushkin, I., et al., *Modeling an inhomogeneous optically thick laser induced plasma: a simplified theoretical approach.* Spectrochimica Acta Part B: Atomic Spectroscopy, 2001. 56(9): p. 1769–1785.

[36] Omenetto, N., J. Winefordner, and C.T.J. Alkemade, *An expression for the atomic fluorescence and thermal-emission intensity under conditions of near saturation and arbitrary*

self-absorption. Spectrochimica Acta Part B: Atomic Spectroscopy, 1975. 30(9): p. 335–341.

[37] Fishman, I., G. Il'in, and M.K. Salakhov, *Spectroscopic diagnostics of a strongly inhomogeneous optically thick plasma. Part 1. The formation of asymmetric self-reversed emission and absorption lines: determination of electron impact half-width and electron concentration.* Spectrochimica Acta Part B: Atomic Spectroscopy, 1995. 50(9): p. 947–959.

[38] Fishman, I., G. II'in, and M.K. Salakhov, *Temperature determination of an optical thick plasma from self-reversed spectral lines.* Journal of Physics D: Applied Physics, 1987. 20(6): p. 728.

[39] Fishman, I., G. Il'in, and M.K. Salakhov, *Spectroscopic diagnostics of a strongly inhomogeneous optically thick plasma. Part 2. Determination of atom concentration and variations of different physical values in the plasma cross-section using asymmetric self-reversed emission and absorption lines.* Spectrochimica Acta Part B: Atomic Spectroscopy, 1995. 50(10): p. 1165–1178.

[40] Karabourniotis, D., *Plasma temperature determination from the maximum intensity of a symmetric self-reversed line.* Journal of Physics D: Applied Physics, 1983. 16(7): p. 1267.

[41] Ilin, G., M.K. Salakhov, and I. Fishman, *Analysis of asymmetric self-reversal of spectral lines for the case of lateral observation of a spectrum.* Zhurnal Prikladnoi Spektroskopii, 1976. 24: p. 201–207.

[42] Lee, Y.-I., et al., *Influence of atmosphere and irradiation wavelength on copper plasma emission induced by excimer and Q-switched Nd: YAG laser ablation.* Applied Spectroscopy, 1997. 51(7): p. 959–964.

[43] Gautier, C., et al., *Main parameters influencing the double-pulse laser-induced breakdown spectroscopy in the collinear beam geometry.* Spectrochimica Acta Part B: Atomic Spectroscopy, 2005. 60(6): p. 792–804.

[44] Rezaei, F. and S.H. Tavassoli, *Quantitative analysis of aluminum samples in He ambient g*as at different pressures in a thick LIBS plasma. Applied Physics B, 2015: p. 1–9.

IntechOpen